Variability in Antarctic Surface Climatology Across Regional Climate Models and Reanalysis Datasets

Jeremy Carter[1], Amber Leeson[2], Andrew Orr[3], Christoph Kittel[4], and J.Melchior van Wessem[5]

[1]Department of Mathematics and Statistics, Lancaster University, Lancaster, United Kingdom
[2]Lancaster Environment Centre, Lancaster University, Lancaster, United Kingdom
[3]British Antarctic Survey, High Cross, Madingley Road, Cambridge, UK
[4]Laboratory of Climatology, Department of Geography, SPHERES, University of Liège, Liège, Belgium
[5]Institute for Marine and Atmospheric Research Utrecht, Utrecht University, Utrecht, Netherlands

Correspondence: Jeremy Carter (j.carter10@lancaster.ac.uk)

Abstract.

Regional climate models (RCMs) and reanalysis datasets provide valuable information for assessing the vulnerability of ice shelves to collapse over Antarctica, which is important for future global sea level rise estimates. Within this context, this paper examines variability in snowfall, near-surface air temperature and melt across products from the MetUM, RACMO and MAR RCMs, as well as the ERA-Interim and ERA5 reanalysis datasets. *Seasonal and Trend decomposition using Loess* (STL) is applied to split the monthly time series at each model grid-cell into trend, seasonal and residual components. Significant, systematic differences between outputs are shown for all variables in the mean and seasonal/monthly standard deviations, occurring at both large and fine spatial scales across Antarctica. Results imply that differences in the atmospheric dynamics, parametrisation, tuning and surface schemes between models together contribute more significantly to large-scale variability than differences in the driving data, resolution, domain specification, ice sheet mask, digital elevation model and boundary conditions. Despite significant systematic differences, high temporal correlations are found for snowfall and near-surface air temperature across all products at fine spatial scales. For melt, only moderate correlation exists at fine spatial scales between different RCMs and low correlation between RCM and reanalysis outputs. Root mean square deviations (RMSDs) between all outputs in the monthly time series for each variable are shown to be significant at fine spatial scales relative to the magnitude of annual deviations. Correcting for systematic differences results in significant reductions of RMSDs, suggesting the importance of observations and further development of bias-correction techniques.

1 Introduction

The largest source of uncertainty in 2100 Sea Level Rise (SLR) projections, for a given Representative Concentration Pathway (RCP), is from the contribution of ice sheets (Kopp et al., 2017). Non-linear instabilities in the Greenland and Antarctic ice sheets give long tails to their SLR probability projections. For example, under RCP 8.5 the median SLR from Antarctica is projected to be of the order of 20 cm, while the 95th percentile is six times higher, at 130 cm (Bamber et al., 2019). The Antarctic continent is fringed by ice shelves, which act like 'ice dams', slowing down the flow of inland ice towards the sea

(Rignot et al., 2004; Scambos et al., 2004). The stability of the ice shelves under a warming climate strongly determines the rate of SLR from Antarctica and it is, in part, the difficulty of modelling their complex physical dynamics, leading to retreat/collapse, that results in the large uncertainty in estimates of future SLR (Bulthuis et al., 2019).

The primary method of ice shelf retreat, when considered across the entire ice sheet, is currently through oceanic basal melting (Pritchard et al., 2012; Paolo et al., 2015), although notable exceptions are recent and dramatic collapse events, such as the disintegration of the Larsen B ice shelf in 2002, which are linked to anomalous atmospheric conditions through the process of melt-induced hydrofracture (Scambos et al., 2000; van den Broeke, 2005; Bell et al., 2018). Anomalously high near-surface air temperatures (leading to enhanced melt events), as well as low accumulation (leading to reduced pore space of surface snow), result in greater lateral propagation of melt water into crevasses across the ice shelf, which then deepen due to increased hydrostatic pressure (Kuipers Munneke et al., 2014). This process reduces the structural integrity of the ice shelf and, in addition to fractures created through supraglacial lake filling and drainage, can eventually lead to collapse (Banwell et al., 2013; Kuipers Munneke et al., 2014). Recent ice sheet modelling studies indicate the critical importance of atmosphere-driven hydrofracture events in distant-past SLR variation (Pollard et al., 2015) and near-future 2100-2300 SLR estimates, particularly under high-emission scenarios (DeConto et al., 2021). Comprehensive spatiotemporal estimates of near-surface air temperature over Antarctica, as well as the accumulation of snowfall and quantity of melt water, are thus important for SLR predictions and are typically provided by RCMs (van Wessem et al., 2018; Agosta et al., 2019; Mottram et al., 2021).

RCMs are limited-area, physically-based, nested models driven at the boundaries by lower-resolution Global Climate Models (GCMs) or reanalysis datasets. The high-resolution available from RCMs is important for capturing fine-scale climatic processes in regions of complex topography, such as föhn winds that occur over ice shelves on the Antarctic Peninsula (Luckman et al., 2014). The region-specific domain enables the set-up and physical schemes of the RCM to be polar optimised (Orr et al., 2021). In addition, further added-value of RCMs is provided through inclusion of region-specific, sophisticated, surface and sub-surface schemes that capture processes such as melt water percolation (Ettema et al., 2010; Datta et al., 2019; Walters et al., 2019). Despite these features, RCMs still exhibit significant systematic errors precluding their direct interpretation in Climate Change Impact Studies (CCIS) (Christensen et al., 2008; Ehret et al., 2012).

The atmospheric model dynamics, surface scheme, parametrisation, driving data, boundary conditions, domain, resolution and orography are all examples of components that contribute to systematic error (Ehret et al., 2012; Giorgi, 2019; Mottram et al., 2021). This paper examines the magnitude and spatial distribution of systematic differences in an ensemble of RCM simulations for Antarctic-wide, 1980-2018 estimates of snowfall, near-surface air temperature and melt water. The relative contribution from different components of the simulations, such as the atmospheric model physics, are discussed. Comparisons of Antarctic-wide RCM simulations of recent-historic surface climatology are present in the literature (Mottram et al., 2021; van Wessem et al., 2018; Agosta et al., 2019), although the focus is predominantly on Surface Mass Balance (SMB). Surface melt flux, when integrated over the Antarctic ice sheet, only represents a small fraction of the total SMB, which is determined predominantly by the flux of snowfall (Lenaerts et al., 2012b; Agosta et al., 2019). This paper provides the first inter-comparison of recent-historic Antarctic-wide RCM simulations framed within the context of ice shelf instability and collapse events, giving specific focus to variability in near-surface air temperature, snowfall and melt water.

Six Antarctic-wide RCM simulations are compared, two from each of the Met Office Unified Model version 11.1 (MetUMv11.1), the Modèle Atmosphérique Régional version 3.10 (MARv3.10) and the Regional Atmospheric Climate Model version 2.3p2 (RACMOv2.3p2). Comparisons are also made to the reanalysis driving data of ERA-Interim and ERA5. The resulting eight Antarctic-wide datasets analysed in this paper are given in Table 1. MARv3.10 and RACMOv2.3p2 are both hydrostatic models specifically developed for use over polar regions and their output from Antarctic-wide simulations have been rigorously compared to one-another and against observations (Lenaerts et al., 2012b; van Wessem et al., 2018; Agosta et al., 2019). The MetUMv11.1 is not specifically developed with a focus on the polar regions, although it is a non-hydrostatic model meaning it can be run at and simulate atmospheric circulation features at sub-kilometer resolutions (Orr et al., 2021), whereas MAR and RACMO are limited to maximum resolutions of 5-10 km horizontal grid spacing (van Wessem et al., 2016; Datta et al., 2019). Another feature of particular note in the MetUM simulations is that a 'zero-layer' surface scheme is used, which has been identified as a major deficiency in simulations compared with the multi-layer schemes included in MAR and RACMO due to impacts such as that on heat transfer and not representing the insulating properties of the column of snow (Slater et al., 2017; Walters et al., 2019). It is therefore expected that the MetUM, as well as the reanalysis datasets ERA-Interim and ERA5 that both use a single tile to represent snow, will produce much less physically realistic evaluations of melt than MAR and RACMO. Further details on key differences in the model specifications for the simulations analysed in this paper are presented in section 2.

Historic, evaluation simulations are chosen to remove dependency on emission scenarios, which have been shown to introduce divergent trajectories of variables such as melt (Trusel et al., 2015; Gilbert and Kittel, 2021; Kittel et al., 2021). Comparisons to observations are not included due to the sparse nature of observations available over Antarctica. Papers including observations typically require comparisons to be made across elevation bins (Mottram et al., 2021; van Wessem et al., 2018; Agosta et al., 2019). In this paper comparisons are made at a 12 km grid-cell level and it is shown that variability between the simulations has greater dependency on the (latitude, longitude) location than elevation. To study the temporal dependence of variability time series decomposition is applied, separating the signal at each location into an annual, seasonal and residual component. These components are driven by different physical processes and the previous inter-comparison papers cited have not focused on examining variability at different temporal scales. Finally, despite the primary motivation for this paper focusing on surface climatology over ice shelves, the analysis is extended to the whole Antarctic ice sheet and surrounding Southern Ocean. This is done to aid discussion, as surface climatology over the ice shelves is influenced by the behaviour of the models over the rest of the domain, and extending the analysis provides insights useful for studies not only focused on ice shelves, thus increasing the scope of the work.

2 Reanalysis Datasets and RCMs Specifications

The ensemble of Antarctic-wide RCM simulations examined in this paper are part of the Coordinated Regional Climate Downscaling Experiment (CORDEX: https://cordex.org/), which is a global project that provides coordinated sets of RCM simulations worldwide. The model specifications for each of the RCM simulations in the chosen ensemble, as well as for the

RCM/Reanalysis Dataset	Domain	Driving Data	Time Period of Forcing [hours]	H.Resolution [km]	Label
ERA-Interim	Global	-	-	79	ERAI
ERA5	Global	-	-	31	ERA5
MetUMv11.1	Antarctica	ERA-Interim	12	12	MetUM(011)
MetUMv11.1	Antarctica	ERA-Interim	12	49	MetUM(044)
MARv3.10	Antarctica	ERA-Interim	6	35	MAR(ERAI)
MARv3.10	Antarctica	ERA5	6	35	MAR(ERA5)
RACMOv2.3p2	Antarctica	ERA-Interim	6	27	RACMO(ERAI)
RACMOv2.3p2	Antarctica	ERA5	3	27	RACMO(ERA5)

Table 1. The two reanalysis datasets and six RCM simulation outputs compared in the paper. The label with which each simulation is referred to in the paper is given.

ERA-Interim and ERA5 reanalysis products, are detailed here. There are significant differences, with some of the key aspects being the following: different atmospheric dynamics components; different surface schemes; differences in the vertical and horizontal resolutions, with particular interest on the performance of the high-resolution 12 km MetUM simulation against the low-resolution 49 km MetUM simulation; differences in the driving data, with particular interest on the two RACMO and two MAR simulations that are otherwise identical; and differences in the Digital Elevation Models (DEMs) and masks used by each model, with MAR and RACMO using comparatively similar DEMs, while the MetUM uses a DEM similar to that of ERA5 (Fig. C1).

2.1 ERA-Interim and ERA5

ERA-Interim, produced by the European Centre for Medium-Range Weather Forecasts (ECMWF), is a global reanalysis dataset spanning 1979-2019 with 6-hourly temporal resolution and approximately uniform horizontal resolution of 79 km spacing and 60 vertical levels up to 10 Pa (Dee et al., 2011). Era-Interim was world leading and is included as the specified driving data in the base criteria for the CORDEX simulations but has since been superseded by ERA5, also produced by ECMWF (Hersbach et al., 2020), with a number of ERA5 driven simulations also included in the Antarctic-CORDEX ensemble of RCM outputs. The ERA5 reanalysis dataset uses the updated Cycle 41r2 version of the Integrated Forecast System (IFS) numerical weather prediction (NWP) model, with significant developments to model physics and assimilation methods (Hersbach et al., 2020). It spans 1950-Present with an enhanced single hourly temporal resolution, horizontal resolution of 31 km and 139 vertical levels up to 1 Pa. In addition, ERA5 has uncertainty estimates derived from an ensemble of 10 data assimilations performed at a 3 hourly temporal resolution and horizontal resolution of 63 km. The elevation used by ERA-Interim comes from interpolating the GTOPO30 elevation product (ECMWF, 2009), whereas for ERA5 surface elevation is derived from interpolation of a combination of the SRTM30 elevation product along with other surface elevation datasets (ECMWF, 2016). The coupled surface schemes used for ERA-Interim and ERA5 are the Tiled ECMWF Scheme for Surface Exchanges over Land (TESSEL)

and updated HTESSEL schemes respectively, both use a single tile to represent snow, while one of the major differences is that HTESSEL allows surface runoff (Balsamo et al., 2009).

2.2 MAR

MAR is a hydrostatic RCM, specifically developed for the polar areas (Fettweis et al., 2013). The Antarctic-wide simulations analysed in this paper have a spatial horizontal resolution of 35 km with a vertical resolution of 24 atmospheric levels. Specific details of the atmospheric component of MAR can be found in Gallée and Schayes (1994); Gallée (1995). The atmospheric model is fully coupled to the 1-D SISVAT (Soil Ice Snow Vegetation Atmosphere Transfer) surface scheme (Fettweis et al., 2013, 2017), which uses the Crocus multi-layer surface snow model (Brun et al., 1992) that contains subroutines for processes such as snow metamorphism as well as meltwater runoff, retention, refreezing and percolation. SISVAT does not include a full radiative transfer scheme in snow/ice and surface albedo is parameterised as a function of snow grain properties (Tedesco et al., 2016). The relaxation technique is used to apply LBCs (Lateral Boundary Conditions) from the driving data every 6 hours and spectral nudging is used to constrain the large-scale behaviour in the upper atmosphere. The two Antarctic-wide MAR simulations studied in this paper are identical apart from differing driving data from ERA-Interim and ERA5 respectively. The orography used in the simulations is from BEDMAP2 (Fretwell et al., 2013). For further detail on MAR and the specific version used to generate the output examined in this paper (MARv3.10) the reader is referred to Agosta et al. (2019) and Mottram et al. (2021).

2.3 RACMO

RACMO is a hydrostatic RCM with a polar version developed to represent the climate specifically over ice sheets (Van Meijgaard et al., 2008). The RCM uses the dynamical core from HIRHAM (High Resolution Limited Area Model) (Undén et al., 2002) and the physics package CY33r1 version of the Integrated Forecast System (IFS) NWP model from ECMWF. The Antarctic-wide simulations analysed in this paper have a spatial horizontal resolution of 27 km with a vertical resolution of 40 atmospheric levels. The simulations include a multi-layer snow scheme that simulates hydrological processes such as melt, percolation, refreezing and runoff as well as firn densification (Ettema et al., 2010). In addition, a drifting snow scheme simulates movement of snow from surface winds across the ice sheet (Lenaerts et al., 2010, 2012a). A snow albedo scheme is implemented, which uses snow grain size as a prognostic variable as well as cloud optical thickness and solar zenith angle to estimate albedo (Munneke et al., 2011). The relaxation technique is used to apply LBCs from the driving data every 6 hours for the RACMO simulation driven by ERA-Interim and every 3 hours for the simulation driven by ERA5 and spectral nudging is used to constrain the large-scale behaviour in the upper atmosphere. The two simulations studied are identical apart from differing driving data from ERA-Interim and ERA5 respectively. The orography used in the simulations is the same as from Bamber et al. (2009). For further detail on RACMO and the specific version used to generate the output examined in this paper (RACMOv2.3p2) the reader is referred to van Wessem et al. (2018) and Mottram et al. (2021).

2.4 MetUM

The MetUM is a non-hydrostatic climate model, not specifically developed or optimised for use over the polar regions but adapted in these simulations for use over Antarctica (Orr et al., 2021). The Regional Atmosphere physics configuration for mid-latitudes (RA1M) is used (Bush et al., 2020), which is identified as the most suitable configuration available for simulating near-surface climatology over Antarctica (Gilbert et al., 2020, 2021). The Joint UK Land Environment Simulator (JULES) (Walters et al., 2019) is used with the option of a comparatively simple zero-layer snow/soil composite scheme that does not capture processes such as refreezing of melt water (Best et al., 2011). The two Antarctic-wide MetUM simulations analysed in this paper are identical apart from their spatial horizontal resolutions of 12 km and 49 km respectively, both have a common vertical resolution of 70 atmospheric levels. These limited-area, regional simulations are nested inside the global model configuration of the MetUM, which is itself forced using ERA-Interim reanalysis data and follows a 12 hour re-initialisation procedure that constrains the large-scale circulation in the interior of the domain and prevents it from drifting too far from the driving data (Gilbert et al., 2021). The global MetUM model runs for 24 hour periods, with a re-initialisation happening throughout the domain every 12 hours and boundary conditions for the nested run saved each hour. The first 12 hours of each 24 hour run is discarded as spin-up, while the second 12 hours of each run is kept as output and stitched together with following runs. The orography used in the simulations is the MetUM standard GLOBE 1 km dataset (Elvidge et al., 2019).

3 Comparison Method

The RCM simulations examined in this paper all use an equatorial rotated coordinate system, where a quasi-uniform horizontal-resolution grid is defined over the region by first specifying the grid over the equator with constant latitude and longitude spacing between each grid-cell and then applying a rotation that takes the domain over the region of interest, for example Antarctica. Direct comparisons between the model output are made by regridding onto a common grid, with a common domain and spatiotemporal coordinates. Cubic precision Clough-Tocher interpolation (Mann, 1999) is performed on the unrotated 'grid latitude' and 'grid longitude' coordinates, which are assumed approximately euclidean, to regrid all model outputs onto the MetUM(011) resolution grid. This grid is chosen as it is the highest resolution grid of the simulations examined, meaning no information is lost as part of the regridding. The domain is filtered to only include the regions common across the model outputs, see Fig. 1. The time series examined is filtered to the common 1981-2018 period and 3/6 hourly outputs are aggregated to monthly averages, which captures the dominant annual and seasonal dependency in the variability. For surface air temperature, filtering to only the common timestamps across the models is first applied and then the average temperature over each month computed. The common timestamps are limited by ERA-Interim to 00 h, 06 h, 12 h and 18 h. This is not required for snowfall or melt, which are defined as fluxes in the model output.

To study annual, seasonal and monthly variability separately, *Seasonal and Trend decomposition using Loess* (STL) (Cleveland et al., 1990) is applied to the time series of each variable at each grid-cell. This results in individual trend (T), seasonal (S) and residual (R) components. The decomposition is additive, meaning for each data point ν=1 to N, the components are summed to give the original time series (Y) (eq.[1]). The trend component represents the low-frequency/long-timescale pat-

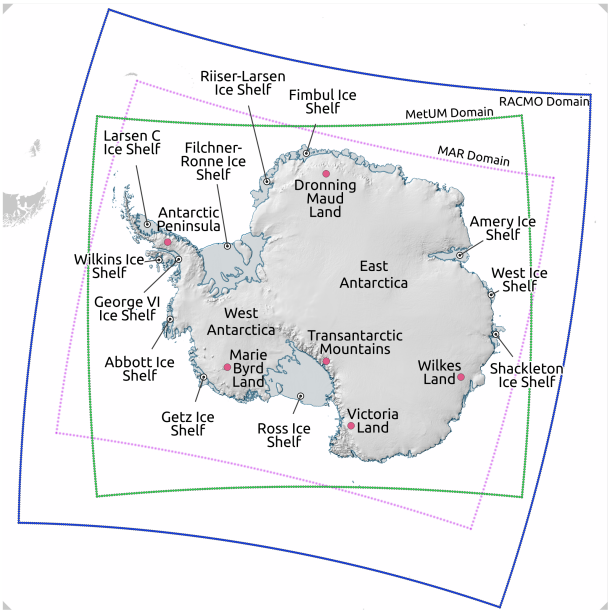

Figure 1. Map of Antarctica with some of the main regions and ice shelves labelled, made using the Quantarctica mapping environment (Matsuoka et al., 2021). The RCM simulation domains for the MetUM (green), RACMO (blue) and MAR (purple) are shown. A 1 km resolution hill-shade has been applied from BEDMAP2 (Fretwell et al., 2013).

tern of the time series, after filtering out medium and high-frequency signals including the seasonal component, which captures periodic patterns, and the residual component that explains fluctuations not caused by the long-scale trend or periodicity in the time series.

$$Y_\nu = T_\nu + S_\nu + R_\nu \tag{1}$$

Basic time series decomposition involves first approximating the trend component by applying a polynomial fit through the data. Subtracting this component gives the de-trended data that is then split into seasonal sub-series (e.g. January, February, ...) and an average of each sub-series gives the seasonal component of the data. Subtracting both the trend and seasonal components then gives the residual component of the series. STL is a more sophisticated procedure that allows options such as robust fitting (where the influence of outliers is limited) and also a time-varying seasonal component. The algorithm is iterative and involves two loops: the outer loop reduces the influence of outliers by assigning weights based on the magnitude of the remainder term; the inner loop involves estimation of the trend and seasonal components through iterative feedback (Cleveland et al., 1990).

The seasonal component is allowed to vary smoothly over the time series, which is done by applying a LOESS (LOcal RegrESSion) smoothing to the monthly sub-series with window length n_s. As $n_s \to \infty$ the LOESS smoothing becomes equivalent to simply taking the average over the sub-series. The value of n_s is recommended to be greater than 7 (Cleveland et al., 1990).

As the value increases, the seasonal component approaches a constant periodic state. In this work 13 is used as this allows potential decadal oscillations in the climate to be captured in the seasonal component, such as the Pacific Decadal Oscillation (PDO).

The trend component is estimated using LOESS with a window of default size (n_t) given by the smallest odd integer greater than the value in eq.[2], which for a period (n_p) of 12 months and seasonal smoother (n_s) of 13 gives $n_t = 21$. This means the seasonal component can be thought of as a 12 month periodic signal that is allowed to change gradually over a 13 year period, while the trend component can be thought of as similar to the result of taking a weighted moving average of the deseasonalized time series over a 21 month period. The residual component is then the remaining signal not described by either the smoothly varying seasonal cycle or the long-timescale trend. An example of applying STL decomposition to the time series of snowfall, surface temperature and melt for a grid-cell on the Larsen C ice shelf is available in section A of the appendix.

$$n_t \geq \frac{1.5 n_p}{1 - 1.5 n_s^{-1}} \tag{2}$$

In this paper temporal variability between the ensemble of Antarctic-wide datasets is assessed in several ways, including: calculating the Pearson linear correlation coefficient between the outputs for each component of the time series and each variable of interest; quantifying differences in the mean of the time series as well as in the standard deviation of the seasonal and residual components; and calculating the root mean square deviation (RMSD) between the outputs for each variable of interest. Each metric is calculated for every grid-cell in the domain, with Antarctic-wide plots showing spatial patterns. Differences in the monthly mean and standard deviation of the components are calculated over the 37 year 1981-2018 period. For snowfall and melt, differences at each grid-cell are expressed as a proportion of the respective inter-annual deviations, providing some measure of the relative significance of differences at each location. The impact of systematic differences in snowfall and melt on estimates of ice shelf stability depend not only on absolute magnitudes but also on the relative magnitude against a baseline variance. The inter-annual, baseline deviation at each grid-cell is approximated as the ensemble average standard deviation in the trend component of the time series. Results presented in spatial maps then show the relative significance of systematic differences and are not simply dominated by the sites with the highest magnitude snowfall/melt.

4 Results

Variability in the ensemble of Antarctic-wide outputs (Table 1) for the monthly time series of snowfall, near-surface air temperature and melt are quantified across the domain through the evaluation of metrics including the correlation between the outputs, systematic differences in the mean and seasonal/residual standard deviations as well as the RMSDs between outputs. These metrics, for variability in the time series, are evaluated at each grid-cell and the main results shown in sections 4.1, 4.2 and 4.3. Spatial maps are used to show large and small scale patterns in the metrics across the domain. Discussion around the results, including features of variability and the relative importance of contributing factors, is given in section 5.

4.1 Correlation

Results are presented for the correlation in the deseasonalized and detrended, residual component of the time series between each of the 28 unique model output pairs. The correlation is computed at every grid-cell and for melt, grid-cells where the ensemble 40-year average monthly melt is less than 1 millimeter water equivalent per month ($mm\ w.e.\ m^{-1}$) are masked as these regions only experience sporadic and insignificant magnitude melt events, essentially equating to numerical noise in the simulations. The average grid-cell correlation across the entire ice sheet is then taken and the results given in Fig. 2. High correlation is shown for snowfall (>0.80) and near-surface air temperature (>0.90) across all model pairs, while results for melt show a significant divide between the reanalysis datasets and the RCMs. The correlation for melt between just the RCMs is moderate to high (>0.55) across all pairs, while for the reanalysis datasets the correlation is low (<0.35) for comparisons to all other models, including between ERA-Interim and ERA5. Another key feature includes the comparatively high correlation shown in every variable between simulations of the same RCM but differing resolution/driving data (MetUM(044)-MetUM(011), MAR(ERAI)-MAR(ERA5) and RACMO(ERAI)-RACMO(ERA5)).

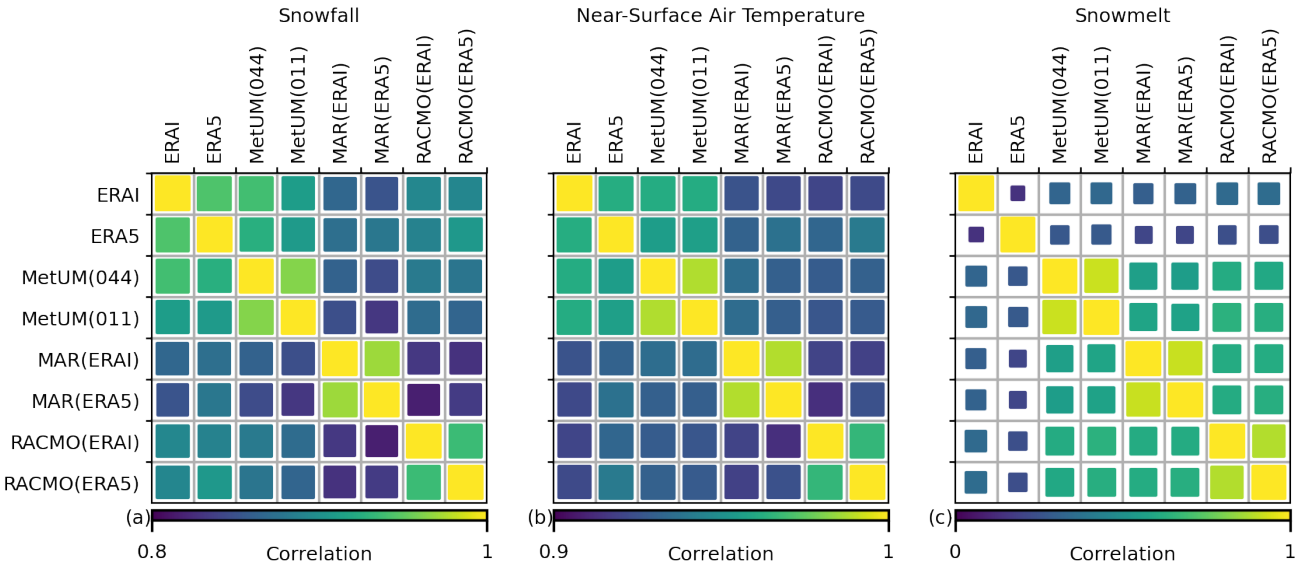

Figure 2. The correlation for snowfall (a), near-surface air temperature (b) and melt (c) between models averaged over the ice-sheet. The colour scale relates to the value of correlation and the scale is adjusted for each plot. The size of each square also relates to the value of correlation, although is kept constant across the figures, going from 0-1, to make comparisons clear between the different variables.

A spatial map of the median correlation in the residual component across the 28 unique model output pairs is plot in Fig. 3. An ice sheet-only mask is applied for melt using the high resolution shapefile from Depoorter et al. (2013), which is found to remove the most prominent edge effects caused by comparing high- and low-resolution models for a variable that is dependent on the sea/ice categorisation of the grid-cell. In addition, grid-cells where the ensemble 40-year average melt is less than 1

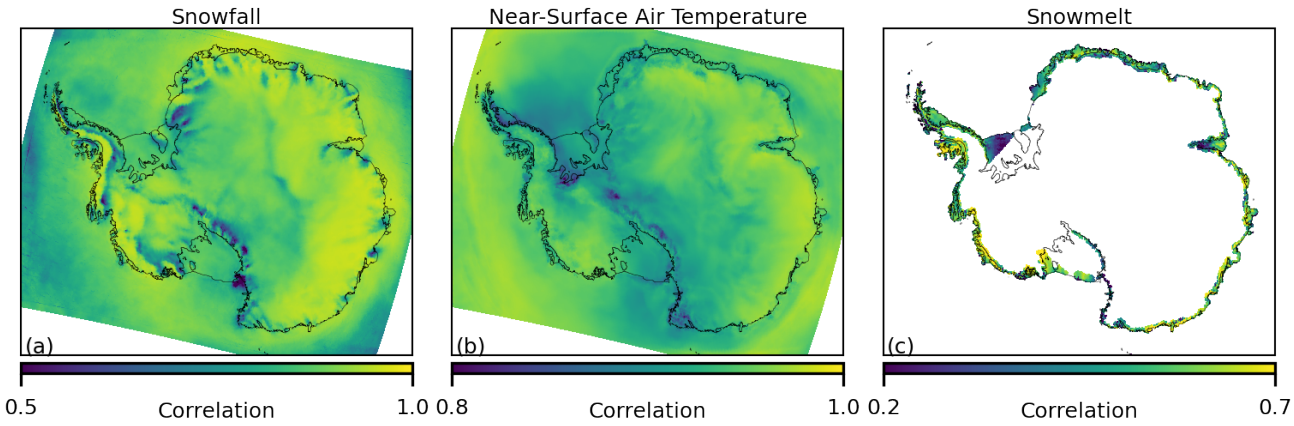

Figure 3. The median correlation by grid-cell in the residual component of the monthly time series between the 28 unique model pairs for snowfall (a), near-surface air temperature (b) and melt (c). The colour scale relates to the value of correlation and the scale/limits are adjusted for each plot.

millimeter water equivalent per month ($mm\ w.e.\ m^{-1}$) are again masked. In Fig. 3 the median correlation for near-surface air temperature is shown to be high (>0.8) across the ice sheet, while for snowfall the correlation remains high again across the majority of the ice sheet but is moderate to low over regions such as the Transantarctic mountains, where the topography varies sharply. For melt, the correlation is moderate over the majority of ice shelves, although is noticeably low over the Ronne ice shelf, the ice shelves bounding Victoria Land, and the interior of the Amery ice shelf.

4.2 Mean and Standard Deviation: Magnitude and Spatial Pattern of Differences

The 1981-2018 mean and standard deviation for each component of the monthly time series of the ice sheet total snowfall, average near-surface air temperature and total melt are displayed in Table 2. Results show that even aggregated across the entire ice sheet significant systematic differences exist between the outputs for each variable. For example, the magnitude of differences in the mean across the ensemble are comparable in magnitude to the average trend standard deviation, which represents inter-annual variations. One particularly striking feature is the contrast between the low monthly melt of ERA5 (1.1 GT/month) compared to the high monthly melt of ERA-Interim (15.5 GT/month) and all RCMs (9.1-14.2 GT/month). It is noted that the relative magnitudes of standard deviations in each component of the time series depends on the variable and that for temperature and melt the seasonal deviation is dominant, while for snowfall both the seasonal and residual deviations have similar magnitudes. Another feature, is that systematic differences are comparatively low between simulations of the same RCM but differing resolution/driving data (MetUM(044)-MetUM(011), MAR(ERAI)-MAR(ERA5) and RACMO(ERAI)-RACMO(ERA5)) when compared with differences present between the different RCMs.

To understand how systematic differences vary spatially the 1981-2018 mean and seasonal/residual standard deviations for the monthly time series of each variable are also computed at a 12 km grid-cell level. Since it is found that systematic differences

Snowfall / GT	ERAI	ERA5	MetUM(044)	MetUM(011)	MAR(ERAI)	MAR(ERA5)	RACMO(ERAI)	RACMO(ERA5)	Average
Monthly Mean	179.3	225.8	212.4	222.8	234.9	235.6	229.6	231.3	221.5
Trend St.D.	7.1	9.8	9.6	9.8	8.7	8.8	8.6	9.1	8.9
Seasonal St.D.	25.9	34.1	26.8	25.8	38.7	38.8	30.1	31.0	31.4
Residual St.D.	21.8	28.3	28.3	28.9	26.3	26.3	28.0	28.2	27.0
Temperature / K	ERAI	ERA5	MetUM(044)	MetUM(011)	MAR(ERAI)	MAR(ERA5)	RACMO(ERAI)	RACMO(ERA5)	Average
Monthly Mean	-32.6	-33.3	-34.2	-33.9	-32.2	-32.2	-34.0	-33.8	-33.3
Trend St.D.	0.4	0.4	0.4	0.4	0.4	0.4	0.4	0.5	0.4
Seasonal St.D.	9.0	7.7	9.3	9.2	8.7	8.6	8.8	8.7	8.7
Residual St.D.	1.1	1.1	1.0	1.0	1.0	1.0	1.2	1.2	1.1
Melt / GT	ERAI	ERA5	MetUM(044)	MetUM(011)	MAR(ERAI)	MAR(ERA5)	RACMO(ERAI)	RACMO(ERA5)	Average
Monthly Mean	15.5	1.1	13.2	14.2	11.9	12.1	9.3	9.1	10.8
Trend St.D.	2.4	0.4	3.0	3.1	3.3	3.1	2.9	2.7	2.6
Seasonal St.D.	29.3	2.0	25.8	27.0	23.1	23.4	18.5	18.2	20.9
Residual St.D.	5.3	0.8	6.8	6.9	7.0	6.8	7.1	6.7	5.9

Table 2. After aggregating across the ice sheet, the mean and standard deviation for each component of the monthly time series for total snowfall, average near-surface air temperature and total melt are given. Values for snowfall and melt are expressed in units of gigatonnes while values for temperature are expressed in Kelvin.

in the mean and standard deviations are most pronounced between different models in the ensemble, results presented in Fig. 4, 5 and 6 are filtered to only include: ERA5; MetUM(011); MAR(ERA5); and RACMO(ERA5). Differences for each model are then plotted relative to this reduced ensemble average (model-ensemble avg.). Results showing direct comparisons between same/similar model pairs are given in Fig. B1, B2 and B3 in the appendix and include differences in the mean and standard deviations between: ERA-Interim and ERA5; MetUM(044) and MetUM(011); MAR(ERAI) and MAR(ERA5); RACMO(ERAI) and RACMO(ERA5). Differences in the standard deviation of the trend component are excluded from grid-cell level results as it is shown in Table 2 that the relative magnitude against standard deviations in the seasonal and residual components is low. For snowfall and melt, differences at each grid-cell are expressed as a proportion of the respective inter-annual deviations, approximated by the ensemble average standard deviation in the trend component.

In Fig. 4, it can be seen that for snowfall there exists high-magnitude, spatially-coherent systematic differences over both the ocean and ice sheet, particularly in the mean of the time series (Fig. 4a,d,g,j), for each model relative to the ensemble average. A specific example is the strong negative difference in the mean snowfall over the ocean and strong positive difference over the majority of the ice sheet shown by MAR (Fig. 4g). In general, the +ve/-ve sign of the differences in the mean and standard deviations for snowfall over the interior of the ice sheet, over the Transantarctic mountains and over the oceans show a relatively large spatial correlation length scale. In contrast, near the periphery of the ice sheet, the sign of the differences exhibit a smaller correlation length scale. Regions such as the Antarctic Peninsula exhibit direction dependent length scales, with a comparatively large length scale in the latitude direction and a comparatively short length scale in the longitude direction. The magnitude of the differences shown over the ice sheet appear greater over sharply varying topography, such as the Transantarctic mountain

range and the steep coastal slopes of the ice sheet. An exception to this being high magnitude differences also shown in the mean component over the comparatively flat region of the interior of East Antarctica for the MetUM(011) and MAR(ERA5) (Fig. 4d,g).

It can be seen that for snowfall the difference present in the mean of the time series has a similar spatial signature and sign as the difference in the standard deviation of the seasonal and residual components (e.g. Fig. 4g,h,i). Exceptions to this include for example the difference in snowfall from the MetUM(011) relative to the ensemble in the interior of East Antarctica, where despite having a lower mean snowfall the standard deviation in the seasonal component is greater than the average of the ensemble (Fig. 4d and 4e).

As with snowfall, there exists significant differences over both the ocean and land for near-surface air temperature between the models, again particularly in the mean of the time series (Fig. 5). For example, MAR shows a significant positive difference in the mean of the time series over the majority of the ice sheet (Fig. 5g) and a significant negative difference over the majority of the surrounding ocean. The magnitude of differences shown over the ice sheet again appear greater over regions of steep topography, particularly for the MetUM(011) and MAR(ERA5) outputs (Fig. 5d,g). The spatial patterns of differences in near-surface air temperature differ in shape compared to those present for snowfall. In particular, near the edge of the ice sheet there are less positive-to-negative fluctuations with changing longitude and instead the patterns are more parallel to the coastline (Fig. 5d,g). While there are similar spatial patterns between the mean temperature difference and the seasonal standard deviation difference (as for Fig. 4), the sign of the differences in Fig. 5 is in general shown to change, for example over the majority of the ice sheet in Fig. 5d compared with Fig. 5e. In Fig. A1e in the appendix, which gives the temperature profiles from each simulation over an example grid-cell on the Larsen C ice shelf, a colder mean temperature is shown to be the result of similar summer temperatures with more severe winter temperatures.

A land-only mask has been applied for melt in Fig. 6 as well as a filter masking any grid-cells where the ensemble mean average monthly melt is less than 1 $mm\ w.e.\ m^{-1}$. This limits discussion of the patterns in differences of the mean and standard deviations to the peripheral areas, which are predominantly ice shelves. The magnitude of the differences present is, as for snowfall, significant relative to the inter-annual variability of melt at each grid-cell. Unlike for snowfall and near-surface temperature, the relative magnitude of differences across the ensemble in the standard deviation of both the seasonal and residual components of the time series are greater than differences present in the mean of the time series. It is noted that for melt, which occurs primarily over just the summer months, greater values of standard deviation in the seasonal component are expected to represent both/either higher magnitudes over peak months and/or a prolonged melt season. As with near-surface temperature and snowfall there are both short and long spatial length scale patterns. An example of a relatively localised spatial pattern is that of the strong positive difference shown by MAR over the interior of the Amery ice shelf in the mean of the time series, as well as the standard deviation of the seasonal and residual components. An example of a large-scale pattern is that ERA5 shows a considerable negative difference in the mean and standard deviations of melt over the majority of ice shelves.

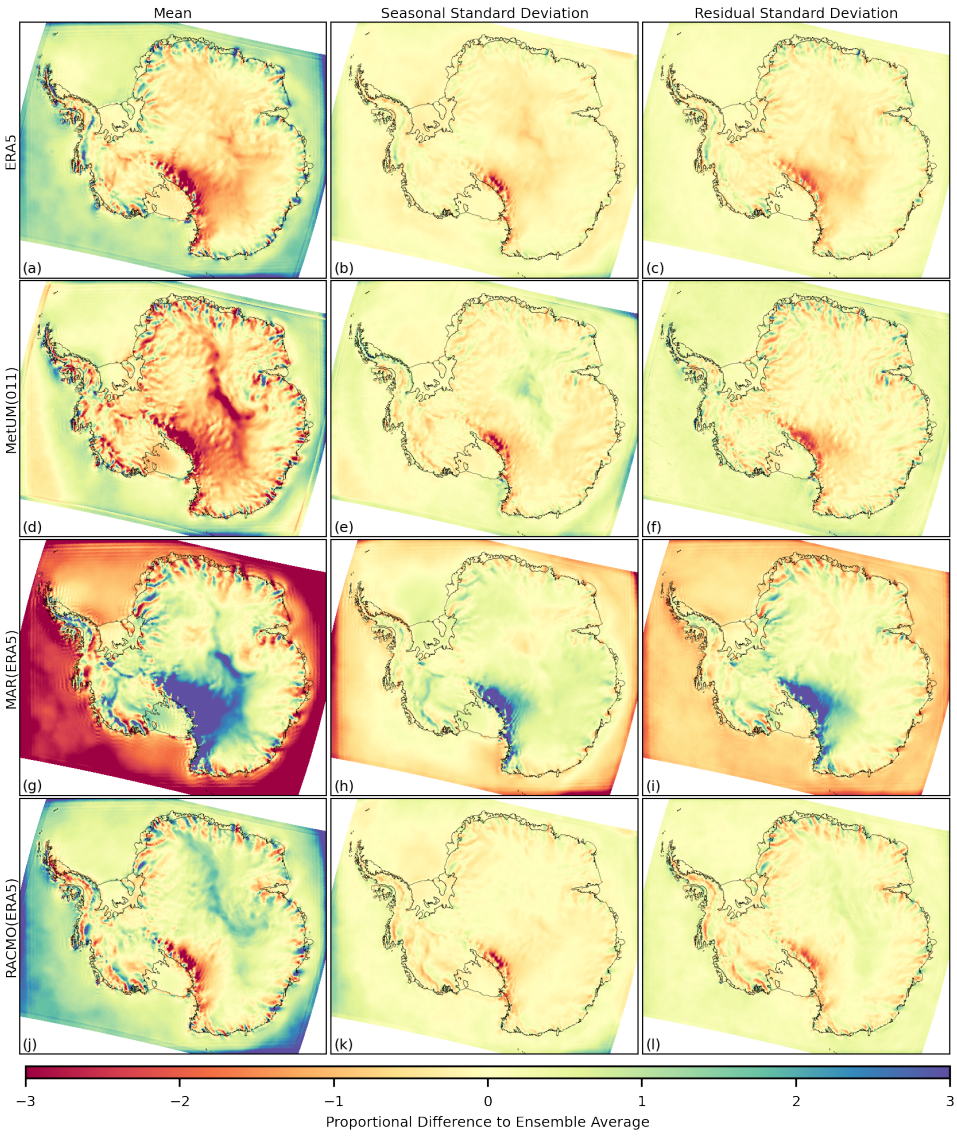

Figure 4. The difference to the ensemble average (model-ensemble avg.) for the 1981-2018 time series of snowfall, in the mean (a,d,g,j), the standard deviation of the seasonal component (b,e,h,k) and the standard deviation of the residual component (c,f,i,l). The ensemble includes: ERA5 (a,b,c); MetUM(011) (d,e,f); MAR(ERA5) (g,h,i); and RACMO(ERA5) (j,k,l). Differences at each grid cell are expressed as a proportion of average inter-annual variation and so do not have units.

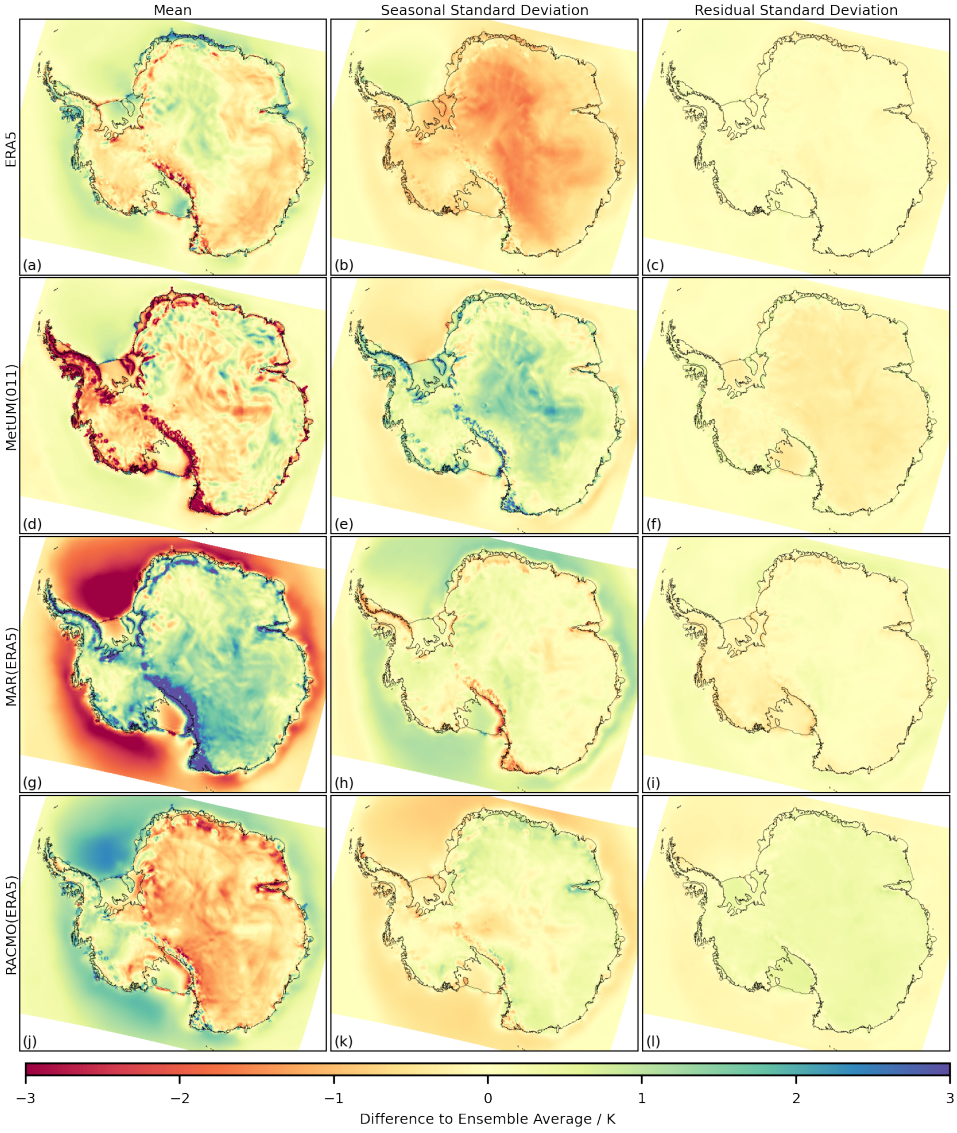

Figure 5. The difference to the ensemble average (model-ensemble avg.) for the 1981-2018 time series of near-surface air temperature, in the mean (a,d,g,j), the standard deviation of the seasonal component (b,e,h,k) and the standard deviation of the residual component (c,f,i,l). The ensemble includes: ERA5 (a,b,c); MetUM(011) (d,e,f); MAR(ERA5) (g,h,i); and RACMO(ERA5) (j,k,l).

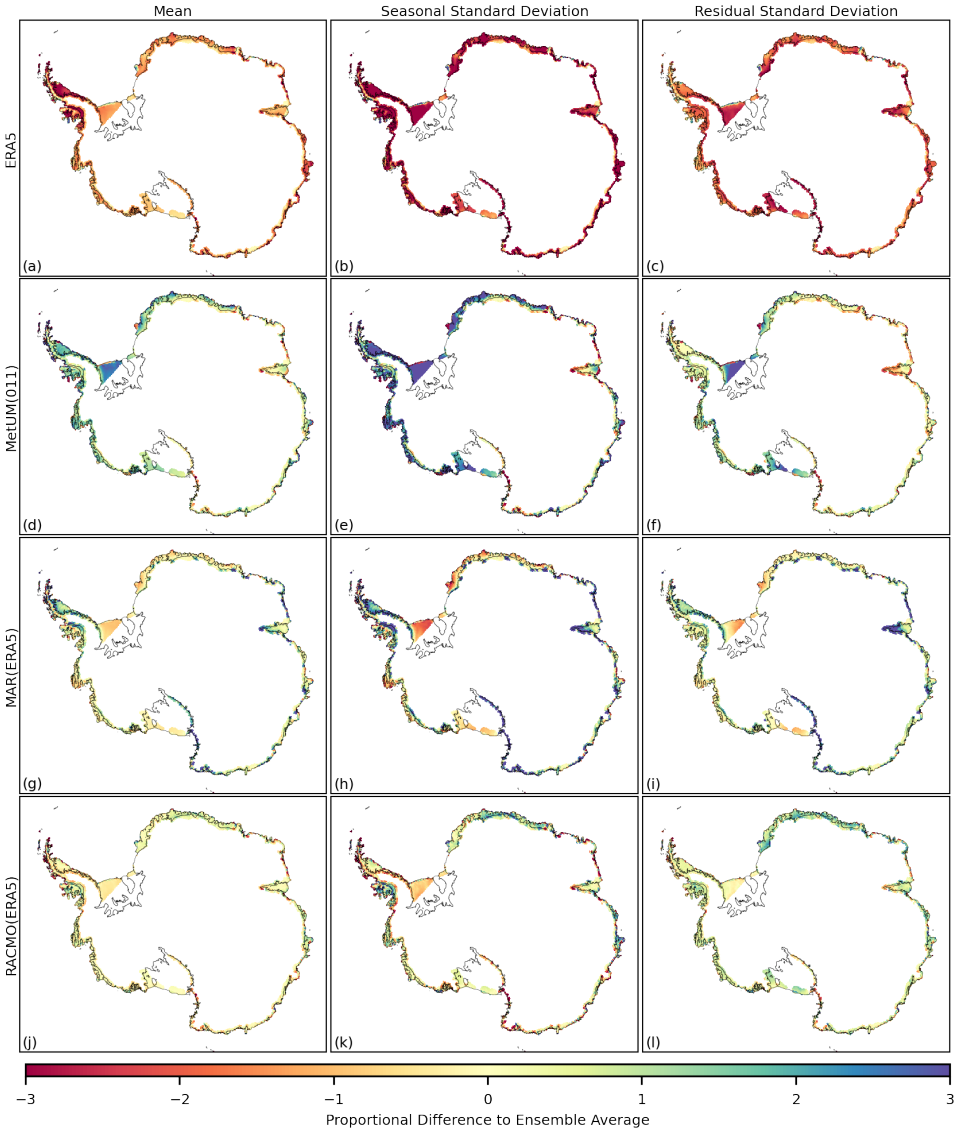

Figure 6. The difference to the ensemble average (model-ensemble avg.) for the 1981-2018 time series of melt, in the mean (a,d,g,j), the standard deviation of the seasonal component (b,e,h,k) and the standard deviation of the residual component (c,f,i,l). The ensemble includes: ERA5 (a,b,c); MetUM(011) (d,e,f); MAR(ERA5) (g,h,i); and RACMO(ERA5) (j,k,l). Differences at each grid cell are expressed as a proportion of average inter-annual variation and so do not have units. Grid-cells where the ensemble mean average monthly melt is less than 1 $mm\ w.e.\ m^{-1}$ are masked.

4.3 RMSD

The RMSD of the monthly time series is evaluated at each grid-cell for each of the 28 unique output pairs of the ensemble. For snowfall and melt, the metric is scaled at each grid-cell by the ensemble average inter-annual standard deviation, described here as the proportional RMSD value. The average is then taken across the ice sheet for each variable and results given in Fig. 7a-c. The average RMSD across the ice sheet provides a measure of the average deviation between the time series of 2 model outputs at each grid cell, while the average proportional RMSD gives a measure of the average relative magnitude of deviations with respect to inter-annual variability. In addition, the percentage reduction in RMSD/proportional RMSD is evaluated after adjusting the mean and seasonal/residual standard deviations at each grid cell for every model output to that of the ensemble average. The average percentage reduction is then taken across the ice sheet for each variable and results given in Fig. 7d-f. This percentage reduction gives a measure of what proportion of the deviations between the time series are the result of systematic differences in both the mean and seasonal/monthly fluctuations.

From Fig. 7 it can be seen the average values for the RMSD/proportional RMSD are significant for all variables, with upper thresholds of 3 K for near-surface air temperature and proportional values of 4 for snowfall and 10 for melt. Values are comparatively low between simulations of the same RCM but differing resolution/driving data (MetUM(044)-MetUM(011), MAR(ERAI)-MAR(ERA5) and RACMO(ERAI)-RACMO(ERA5)) when compared with differences present between the different RCMs. For melt, ERA-Interim has noticeably higher values of proportional RMSD compared to the other models, while for snowfall and temperature differences are less pronounced but the two simulations from MAR show higher average proportional RMSD for snowfall compared with the other models.

The percentage change in RMSD/proportional RMSD after adjusting for equal means and seasonal/residual standard deviations is significant for all variables, as shown in Fig. 7. Upper thresholds on the percentage reduction are 50%, 70% and 60% for snowfall, near-surface air temperature and melt respectively. For melt, the most significant reductions are for ERA-Interim, while ERA5 shows the least significant reductions with proportional RMSD actually increasing between ERA5 and the RACMO products. Across the variables it can be seen that the percentage reduction in RMSD between the high/low resolution MetUM simulation pairs is of greater magnitude than reductions between the two ERA-Interim/ERA5 driven RACMO pairs and two ERA-Interim/ERA5 driven MAR pairs.

5 Discussion

The results presented in this paper show that for all variables studied, when considered across the entire ice sheet, the outputs that came from the same model (MetUM(011/044), MAR(ERAI/ERA5), RACMO(ERAI/ERA5)) exhibit the highest correlations in the time series as well as the smallest systematic differences and RMSDs. This is despite significant differences in resolution between the MetUM runs, which span the highest and lowest resolution RCM simulations made available from the Antarctic-CORDEX project, as well as significant differences in the driving data for the two MAR and RACMO runs. Note that, although ERA5 is an update to ERA-Interim, the results in Table 2 and in section B of the appendix show that the magnitude of systematic differences in the mean and standard deviations between the reanalysis datasets are of similar or

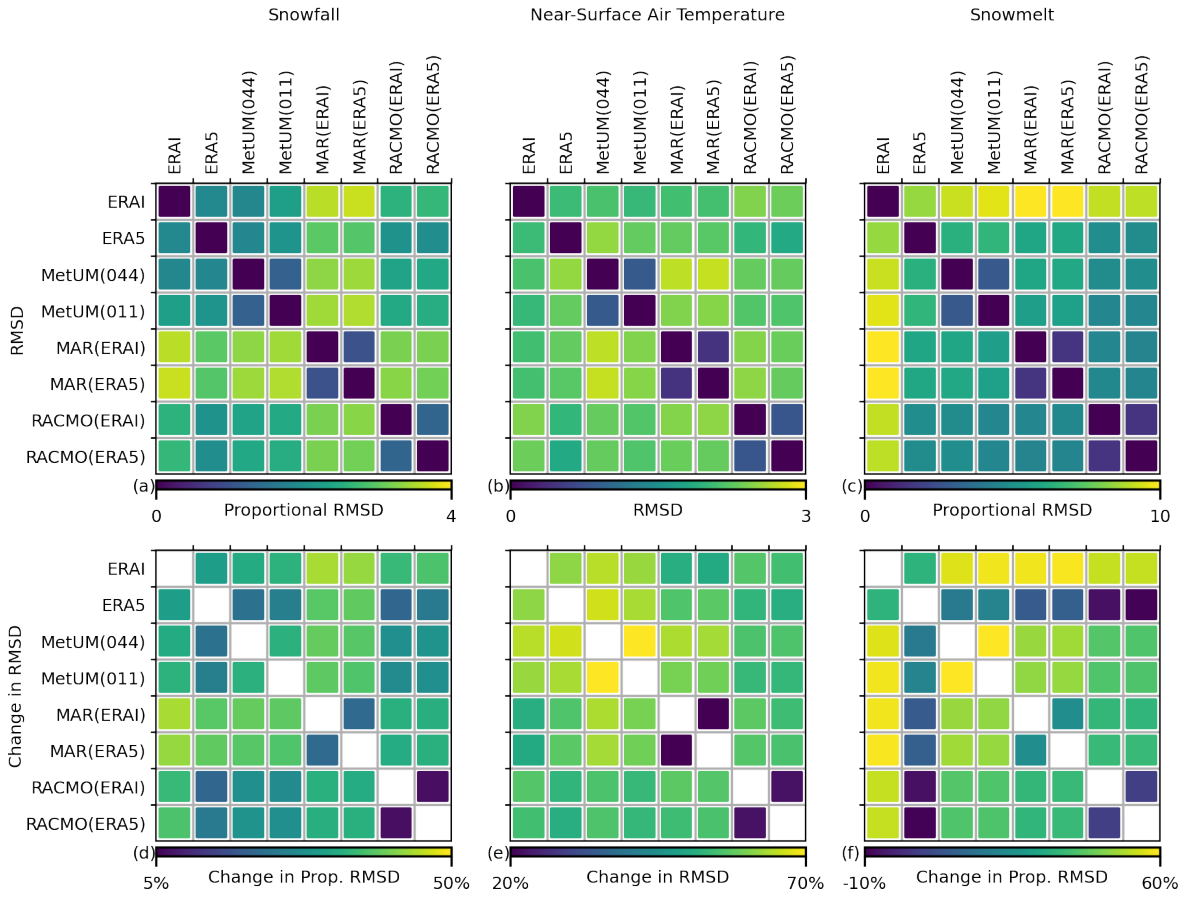

Figure 7. The RMSD/proportional RMSD for snowfall (a), near-surface air temperature (b) and melt (c) between models averaged over the ice-sheet. It is noted for melt that grid-cells where the ensemble average is less than than 1 $mm\ w.e.\ m^{-1}$ are excluded. After adjusting the mean and seasonal/residual standard deviations of all outputs to the ensemble average the percentage reduction in RMSD/proportional RMSD is plot for snowfall (d), near-surface air temperature (e) and melt (f).

greater magnitude to that of differences between different RCM outputs (Fig. 4, 5 and 6). Updates in the model physics and assimilation techniques used by ERA5 (Hersbach et al., 2020) compared to ERA-Interim are hypothesised to be the primary reason for large-scale differences in snowfall and near-surface air temperature identified between the reanalysis outputs. While EAR-Interim and ERA5 exhibit large differences in their DEMs (Fig. C1), it is argued in section 5.1 that differences in DEM are not primary contributors to systematic differences in the models output. The particularly significant difference (over an order of magnitude) for ice-sheet-wide melt between ERA-Interim (15.5 GT) and ERA5 (1.1 GT) is hypothesised to be primarily due to an updated surface scheme (HTESSEL) used in ERA5 that allows run-off (Balsamo et al., 2009).

Results therefore suggest, that differing resolution and driving data are not primary contributors to large-scale spatial variability across the ensemble. Similarity in the spatial and temporal patterns between Antarctic-wide outputs of the same RCM with different driving data agrees with findings from (Agosta et al., 2019), where outputs from MAR are compared with differing reanalysis driving data from ERA-Interim, JRA-55 and MERRA-2. Similarity in results aggregated over the ice sheet (Table 2) between Antarctic-wide outputs of the same RCM with different driving data agrees with findings from Mottram et al. (2021) where SMB for two simulations of differing resolution (12/50 km) for the RCM HIRHAM5 are compared against other RCMs. At finer, more localised scales differing resolution is shown to create significant differences in the mean and seasonal/residual standard deviations for the monthly time series of each variable, see Fig. B1, B2 and B3 (d-f) in the appendix that show direct comparisons between the high- and low-resolution MetUM simulations.

The magnitude of differences in snowfall and near-surface air temperature due to resolution are greatest over regions of sharply varying topography, such as: the Transantarctic mountains; the coastal slopes of the ice sheet; and the Antarctic Peninsula. The representation of atmospheric processes occurring over mountainous regions including foehn winds that occur over the Antarctic Peninsula and katabatic winds occurring over the coastal slopes of East Antarctica are known to be resolution dependent (Orr et al., 2014; Heinemann and Zentek, 2021; Orr et al., 2021). Foehn and katabatic winds have been shown to impact climate over ice shelves, which are often in close vicinity of steep terrain, and are an important driver of surface melt (Bromwich, 1989; Cape et al., 2015; Lenaerts et al., 2017; Datta et al., 2019; Elvidge et al., 2020). In Fig. B2d the difference in the mean near-surface air temperature, due to resolution, extends over ice shelves such as the interior of the Amery ice shelf, which is a well-known katabatic wind confluence zone (Parish and Bromwich, 2007). Despite this influence of resolution on the climatology over ice shelves, greater systematic differences in melt shown in Fig. 6 compared with Fig. B3(d-f) indicate the potentially more significant importance of differences in surface schemes across the particular ensemble of RCMs studied. It is expected that even at 12 km resolution climatically important terrain-induced atmospheric processes, such as foehn/katabatic winds, are not being realistically resolved as is shown in Orr et al. (2021) where output from the MetUM RCM at 4 km, 1.5 km and 0.5 km during a foehn wind event on the Larsen C ice shelf show no obvious convergence towards observations during the event.

The same-model RCM simulations in the ensemble, as well as having identical model physics, parametrisation and tuning, also share factors such as the domain specification, ice mask applied, digital elevation model and boundary conditions. The relative contribution of these additional factors is explored in section 5.1 and from this it is argued that the joint influence of choices in model physics, parametrisation and tuning is the primary factor influencing large-scale variability across the ensemble. The impact of parameter tuning is discussed in Gallée and Gorodetskaya (2008) where it is shown that adjusting the relative contribution of snow particles compared to ice particles in MAR's radiative scheme has a significant impact on near-surface air temperature. A higher relative contribution of snow particles leads to greater flux in long-wavelength downwards radiation. In addition to exploring the relative contribution of different factors to the large spatial scale variability in the ensemble, in section 5.2 specific features of the variability that are mentioned in results section 4 are discussed and the nature of variability for different variables, regions and time-scales is examined.

5.1 Contribution to Variability from the choice of Domain, Ice Mask, Boundary Conditions and DEM

The exact spatial domains differ between the RCM simulations as shown in Fig. 1. However, the spatial domain for all RCM simulations examined is Antarctic-wide and domain boundaries all exist over the ocean, implying there should be no strong local forcing at any of the boundaries. The effect of increasing domain size over the ocean on the output of simulations from MAR over the Greenland ice sheet has previously been studied and found to not significantly impact results over the ice sheet (Franco et al., 2012). In general, the domain size should be great enough such that the buffer zone, in which boundary conditions are applied, does not intersect the region of interest, which in this case is the Antarctic ice sheet. It is found that for the MetUM(044) run, the buffer zone intersects some areas of the periphery of the ice sheet, shown clearly in Fig. B1d. Despite this, it can be seen that effects are localised to the buffer zone boundary, and that even for the regions of the ice sheet that intersect this the relative impact on systematic differences appears less significant than other factors explored. Overall it is assumed that, for the ensemble of RCM simulations studied, differences in the domains does not have a significant effect on the model output for surface climatology over the ice sheet.

As well as having differences in the outer domain boundaries, the different models also have slight differences in the specified boundaries of the ice sheet due to different coordinates and ice masks used. This creates edge effects at the periphery of the ice sheet, particularly noticeable for melt in for example Fig. 5d at the edges of the Ronne-Filchner and Ross ice shelves. It is shown in Mottram et al. (2021) and Hansen et al. (2022) that these edge effects, due to inconsistent ice masks, can have a significant impact on the total estimated SMB over the ice sheet. In this paper, although ice sheet wide totals are computed (Table 2), the focus is primarily on evaluating variability in the time series at each 12 km grid cell after regridding products to a common high-resolution grid. Results for spatial maps of differences for melt are masked using an ice-sheet only mask from Depoorter et al. (2013), which is found to exclude the most significant edge effects from areas where low-resolution models overestimate the extent of the ice sheet after regridding. The same mask is applied before calculating average correlations and RMSDs also reducing the impact of edge effects. Results presented and discussed here, particularly regarding large-scale spatial patterns, are therefore assumed to not be significantly impacted by the different ice masks used in the ensemble of simulations.

Another important consideration when comparing RCM simulations is how the method of applying boundary conditions varies across the ensemble. In particular, although all RCMs examined are nudged at the boundaries within buffer zones, MAR and RACMO also use spectral nudging that constrains the large scale circulation in the interior of domain, while the MetUM instead uses a re-initialisation procedure. Spectral nudging involves applying the relaxation technique throughout the interior of the domain to the long wavelength components of the climate model fields (von Storch et al., 2000). This constrains the large-scale climatology of the RCM output to that of the driving data, while allowing value-added by the RCM in the small-scale features. The same is aimed to be achieved with the re-initialisation of the MetUM throughout the domain every 12 hours, as discussed in section 2.4. The fact that systematic differences between the MetUM, MAR and RACMO are all of significant and comparable magnitude (Fig.4(g,j),5(g,j) and 6(g,j)), despite MAR and RACMO sharing the technique of spectral nudging, suggests that differences between the specific approach of applying large-scale constraints within the ensemble of RCMs

studied is not one of the main features contributing to variability in the mean and seasonal/residual standard deviations of snowfall, near-surface air temperature and melt. It is noted however, that in general the MetUM simulations, rather than the MAR and RACMO simulations, show slightly higher correlation to the reanalysis driving data across the ice sheet for the monthly time series of snowfall and surface temperature (Fig. 2), indicating that the re-initialisation procedure potentially constrains the output across the ice sheet more than spectral nudging.

The differences between DEMs used across the ensemble are plot in Fig. C1 in the appendix. The elevation profiles can be split into three main groups: the coarse elevation profile of ERA-Interim (Fig. C1a); the elevation profiles of ERA5 and the MetUM high- and low-resolution runs (Fig. C1b,c,d); and the elevation profiles of MAR and RACMO (Fig. C1e,f). Differences in the DEMs do not mirror the systematic differences shown in section 4.2. For example, while MAR and RACMO share comparatively similar DEMs, the models do not share similar patterns in systematic differences (Fig. B1, B2 and B3). This indicates differences in the DEMs are not primary contributors to systematic differences in the models output, which is further supported by results displayed in Fig. C2 where weak linear correlation is found between differences in elevation and differences in mean near-surface air temperature.

In this section, features including the domain specification, ice mask applied, digital elevation model and boundary conditions applied are argued to not be the primary contributors responsible for the large-scale systematic differences between the ensemble of model outputs. This result, in addition to the previously discussed secondary contributions of resolution and driving data towards large-scale differences, by way of elimination gives that the joint influence of choices in model physics, parametrisation and tuning is the primary factor influencing large-scale systematic differences across the ensemble.

5.2 Specific Features of the Variability

Specific features in the variability, identified and mentioned in section 4, are discussed here. In section 4.1 it is mentioned that for melt there is a clear divide in the average correlation in the residual component of the time series between reanalysis datasets compared with RCMs (Fig. 2). That is the correlations between different RCMs are greater than between reanalysis datasets and RCM outputs. This is not the case for snowfall and near-surface air temperature, suggesting the divide in correlation for melt is primarily due to differences in the sophistication and polar specific tuning of the surface schemes used for the RCM simulations and the global reanalysis products. It is shown in Hansen et al. (2021) that the subsurface scheme and the handling of layers within the scheme can have a significant impact on melt.

In section 4.1 it is also shown that, particularly for snowfall and melt, the median correlation between the outputs is strongly dependent on the specific region and topography. For melt, three regions are highlighted that show low correlation including the Ronne ice shelf, the ice shelves bounding Victoria Land, and the interior of the Amery ice shelf. In the case of the Ronne ice shelf, the low correlation in melt is due to relatively low average melt occurring over the region, so fluctuations away from no melt are small and erratic. Low correlation over ice shelves bounding Victoria Land is expected to be caused by a combination of their fine scale and the sharply varying topography in the region, making the climatology around them difficult to resolve with the resolution available in the climate models. Finally, the pattern of low correlation around regions such as the interior of the Amery ice shelf is likely the result of atmospheric processes difficult to represent fully in the models, for example: katabatic

winds, driven by gravity, flowing from the interior of the ice sheet to the exterior down elevation channels have a significant impact on the climate on the Amery ice shelf, particularly near the grounding line (Lenaerts et al., 2017).

As with for correlation, the systematic differences shown between the outputs in the ensemble vary depending on the region and topography, see section 4.2. This is true at large and small spatial scales and for all variables. An example of a dependency at large scale is in Fig. 4g where MAR shows a significant positive difference in the 40-year mean monthly snowfall relative to the other outputs over the majority of the ice sheet and a significant negative difference over the majority of the surrounding ocean. In the case of MAR this is hypothesized to be due to a couple of reasons: MAR is forced at the boundaries by humidity and needs time to transform this into precipitation; MAR allows precipitation to be advected through the atmospheric layers until reaching the surface. The advection of precipitation in MAR through each atmospheric layer, in comparison to the instantaneous depositing of precipitation by RACMO, leads to increased snowfall towards the interior of the ice sheet, previously identified in Agosta et al. (2019).

In section 4.3 the RMSD between each model pair, calculated at each grid cell and then averaged across the ice sheet, is presented. This metric of average deviation is dependent on the temporal correlation and presence of systematic differences between the outputs. High values of proportional RMSD for melt, shown in Fig. 7 are the result of relatively low temporal correlations between models as well as relatively high systematic differences. It is noted that for melt, despite there being a clear divide in temporal correlations between reanalysis datasets and RCMs (Fig. 2), the RMSD between ERA5 and the RCMs is of comparable magnitude to values between the RCMs. This is due to particularly low values of total melt exhibited from ERA5 (Table 2) and resulting low magnitude fluctuations of melt. The percentage change in RMSD, after adjusting the mean and seasonal/residual standard deviations of all outputs to the ensemble average, further supports this as it can be seen for melt that ERA5 exhibits the smallest reduction in RMSD after adjustments (Fig. 7). The converse of the above argument is true for ERA-Interim, which shows particularly high values of total melt and so particularly significant values of RMSD and of percentage reductions after adjusting the mean and seasonal/residual standard deviations. Differences in the model outputs for melt across Antarctica remain significant with respect to inter-annual deviations even after adjusting for systematic differences in the mean and standard deviation of the seasonal/residual components of the time series, indicating the importance of improving surface schemes across the models.

6 Conclusions

The spatial nature and magnitude of variability present in an ensemble of current, state-of-the-art Antarctic-wide RCM outputs and global reanalysis datasets is examined for snowfall, near-surface air temperature and melt. This is done at a 12 km grid level, rather than across elevation bins, which reveals significant spatial patterns in correlation and systematic differences in the mean and seasonal/residual standard deviation. Time series decomposition is used to split comparisons across an approximately inter-annual trend component, a periodic seasonal component and a monthly residual component, which is useful for impact assessments where knowledge of variability in the climate data across different time-scales and climate drivers is needed.

It is found that the RCM outputs and reanalysis datasets show high correlation for the monthly time series of snowfall and surface temperature across the majority of Antarctica and the bounding Southern Ocean. Despite this, there exists significant differences, with respect to both magnitude and spatial scale, in the mean and seasonal/residual standard deviations of the time series. In addition, high RMSD between the outputs is found for all variables and is particularly significant for melt with respect to the proportional values relative to annual fluctuations. The primary sources of large-scale, systematic differences between the simulations, for all variables and components, are identified as deriving from differences in the model dynamical core, the surface scheme and the parametrisation and tuning. Differences in driving data, resolution, domains, ice masks, DEMs and boundary conditions are identified as having a secondary contribution. On local, fine spatial scales the relative contribution from different factors is more complex and differences in for example resolution are shown to have a more significant impact.

The variability in snowfall, near-surface air temperature and melt shown is expected to introduce significant uncertainty in estimates of the ice shelf stability with regard to collapse events, which as discussed may have an important contribution to future SLR estimates. It is suggested that the magnitude and scale of systematic differences across the ensemble precludes the direct use and interpretation of individual outputs in impact assessments regarding ice shelf collapse. Results show that removing systematic differences between the ensemble of outputs, significantly reduces the average RMSD. Therefore, as concluded in Mottram et al. (2021), there is an importance on observational campaigns to correct for systematic differences. Improved coverage and quality of observations will provide greater constraints with which to both tune and update the model physics and parametrisations, as well as to use and reduce uncertainties in post-processing bias correction. In addition, further development of RCMs, with particular focus on improvements to the performance of surface schemes over regions of high-melt, is needed to reduce uncertainties around collapse events and future SLR. Finally, it is suggested that further development of sophisticated techniques for bias correction are needed, that are compatible with sparse observations and make use of factors such as the spatial distribution of variability identified in this paper.

Code and data availability. The monthly output from all RCM simulations examined in this paper, as well as the processed data used for figures and tables, is available at: https://doi.org/10.5281/zenodo.6367850 (Carter et al., 2022). The code used to import, process and generate the figures/tables is available at: https://doi.org/10.5281/zenodo.6375205 (Carter, 2022). The reanalysis data is available to download through the C3S climate data store (CDS) (ECMWF, 2011; Hersbach et al., 2018). Further outputs from Antarctic-wide RCM simulations are available from the the Antarctic-CORDEX project: https://climate-cryosphere.org/antarctic/.

Appendix A: STL Decomposition

Figure A1 shows an example of applying STL decomposition to the time series of snowfall, surface temperature and melt for a grid-cell on the Larsen C ice shelf. The decomposition has been applied to each of the 8 model outputs examined in this paper. The trend, seasonal and residual components are shown next to the original time series. Decomposing the time series into these components allows some features to be extracted. For example, in the case of snowfall and surface temperature the models all show high correlation in the inter-annual trend, although there exists a significant systematic difference in the mean between the models. Similarly, for snowfall and surface temperature there is high correlation in the residual term between the models but there is a systematic difference between the models in the standard deviation of that component. In the case of melt, the correlation is more moderate for the trend and residual components, meaning systematic differences are less obvious. The seasonal and residual components in STL decomposition are defined to have approximately zero mean.

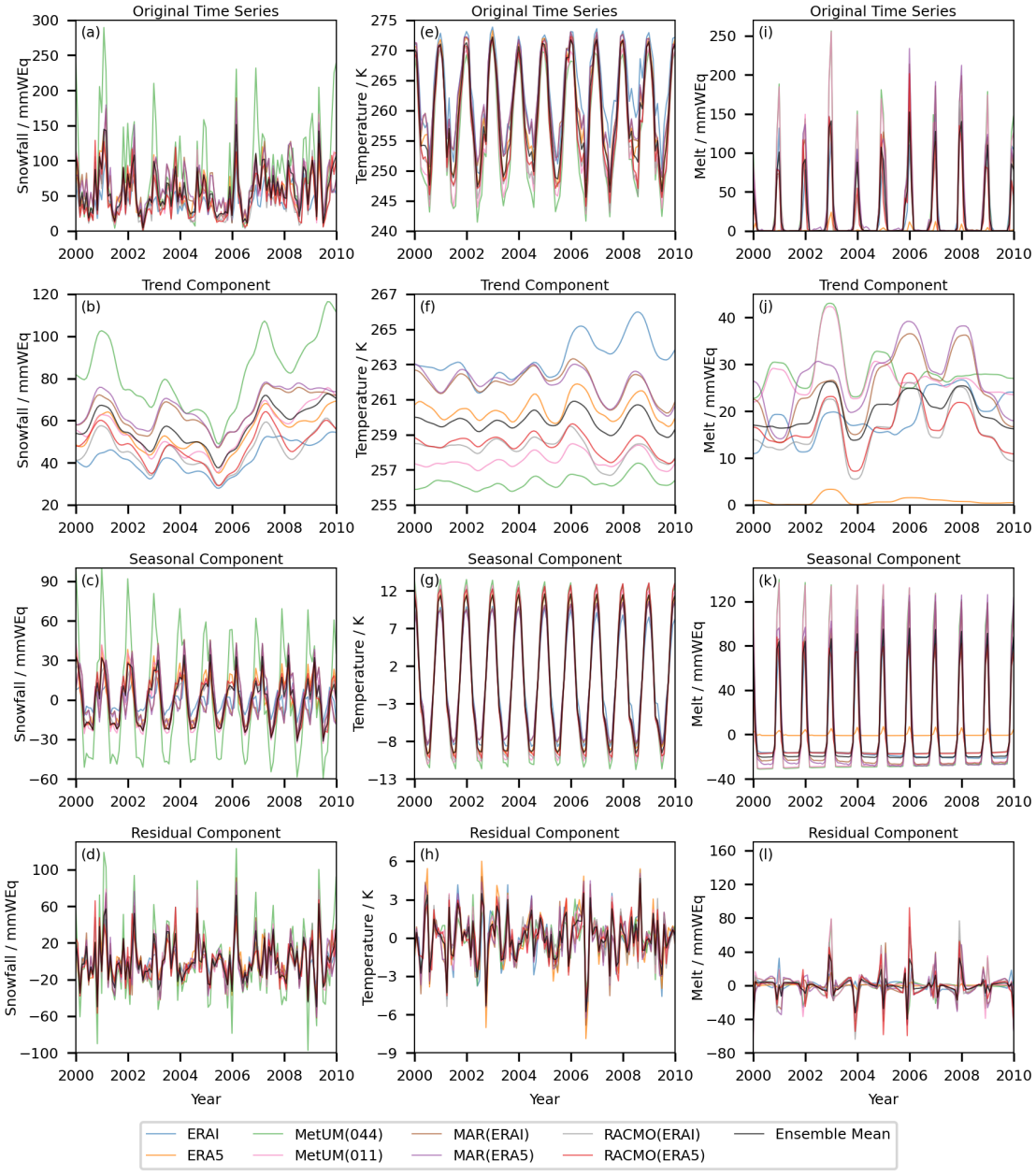

Figure A1. An example of STL decomposition applied to the monthly time series of snowfall (a,b,c,d), surface temperature (e,f,g,h) and melt (i,j,k,l) for a grid-cell near the grounding line on the Larsen C ice shelf. The original time series for the years 2000-2010 are shown (a, e, i), as are the trend (b, f, j), seasonal (c, g, k) and residual (d, h, l) decompositions. The model is additive meaning the sum of trend, seasonal and residual components returns the original time series. Parameter values are $n_s = 13$ and $n_t = 21$.

Appendix B: Same Core Model Differences

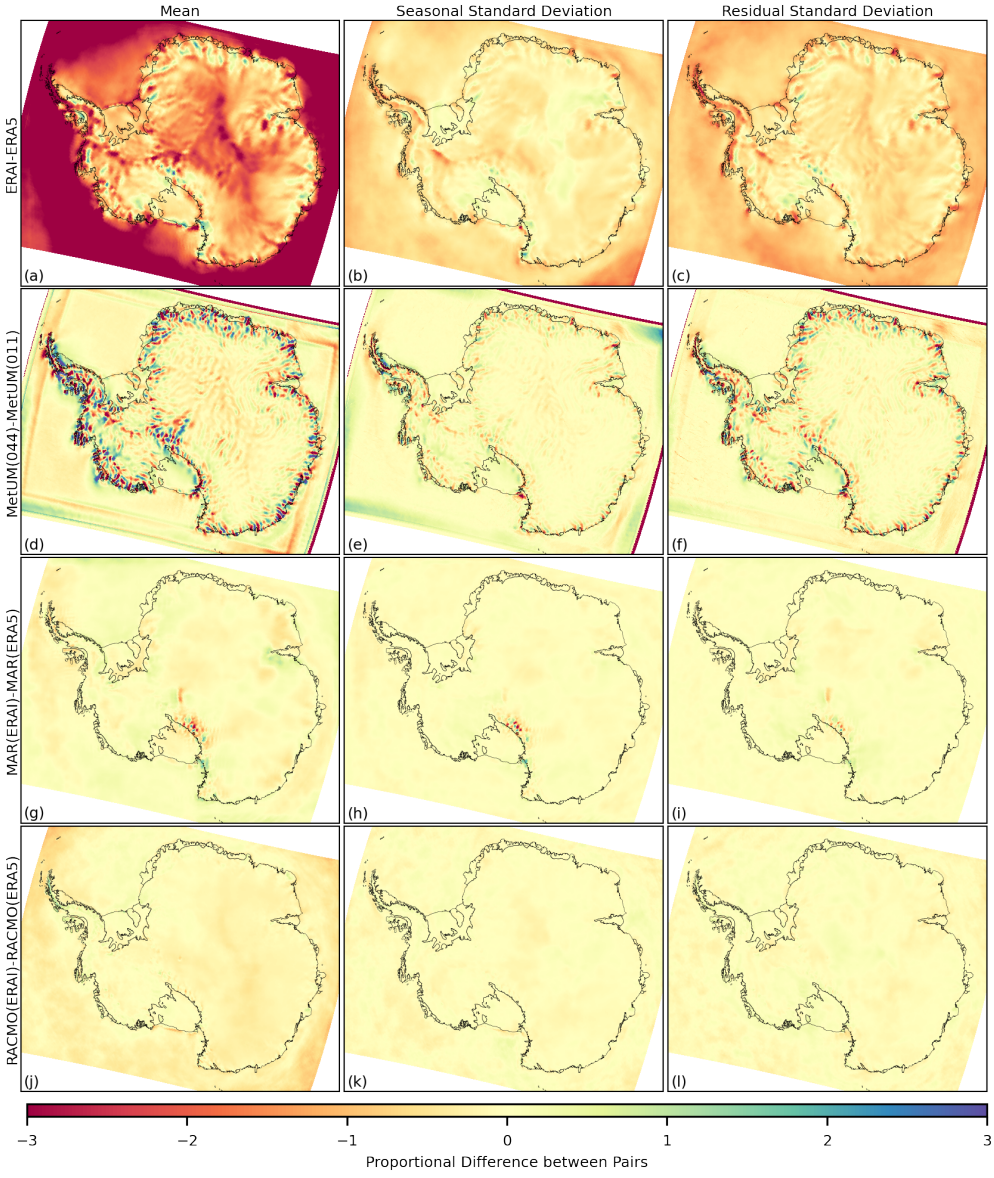

Figure B1. The difference for the 1981-2018 time series of snowfall, in the mean (a,d,g,j), the standard deviation of the seasonal component (b,e,h,k) and the standard deviation of the residual component (c,f,i,l) between the following pairs of outputs: ERA-Interim relative to ERA5 (a,b,c); MetUM(044) relative to MetUM(011) (d,e,f); MAR(ERAI) relative to MAR(ERA5) (g,h,i); RACMO(ERAI) relative to RACMO(ERA5) (j,k,l). Differences at each grid cell are expressed as a proportion of average inter-annual variation and so do not have units.

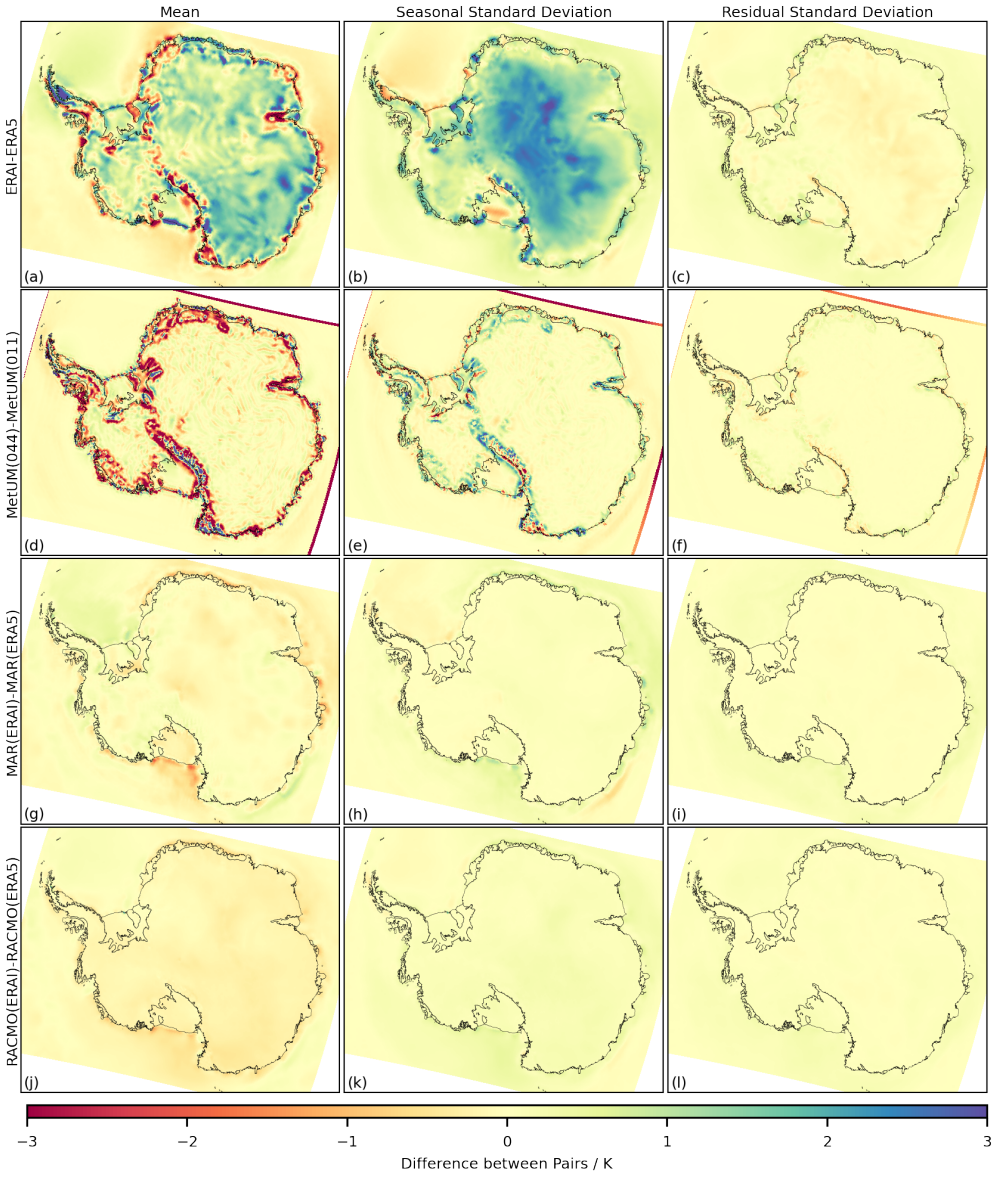

Figure B2. The difference for the 1981-2018 time series of near-surface air temperature, in the mean (a,d,g,j), the standard deviation of the seasonal component (b,e,h,k) and the standard deviation of the residual component (c,f,i,l) between the following pairs of outputs: ERA-Interim relative to ERA5 (a,b,c); MetUM(044) relative to MetUM(011) (d,e,f); MAR(ERAI) relative to MAR(ERA5) (g,h,i); RACMO(ERAI) relative to RACMO(ERA5) (j,k,l).

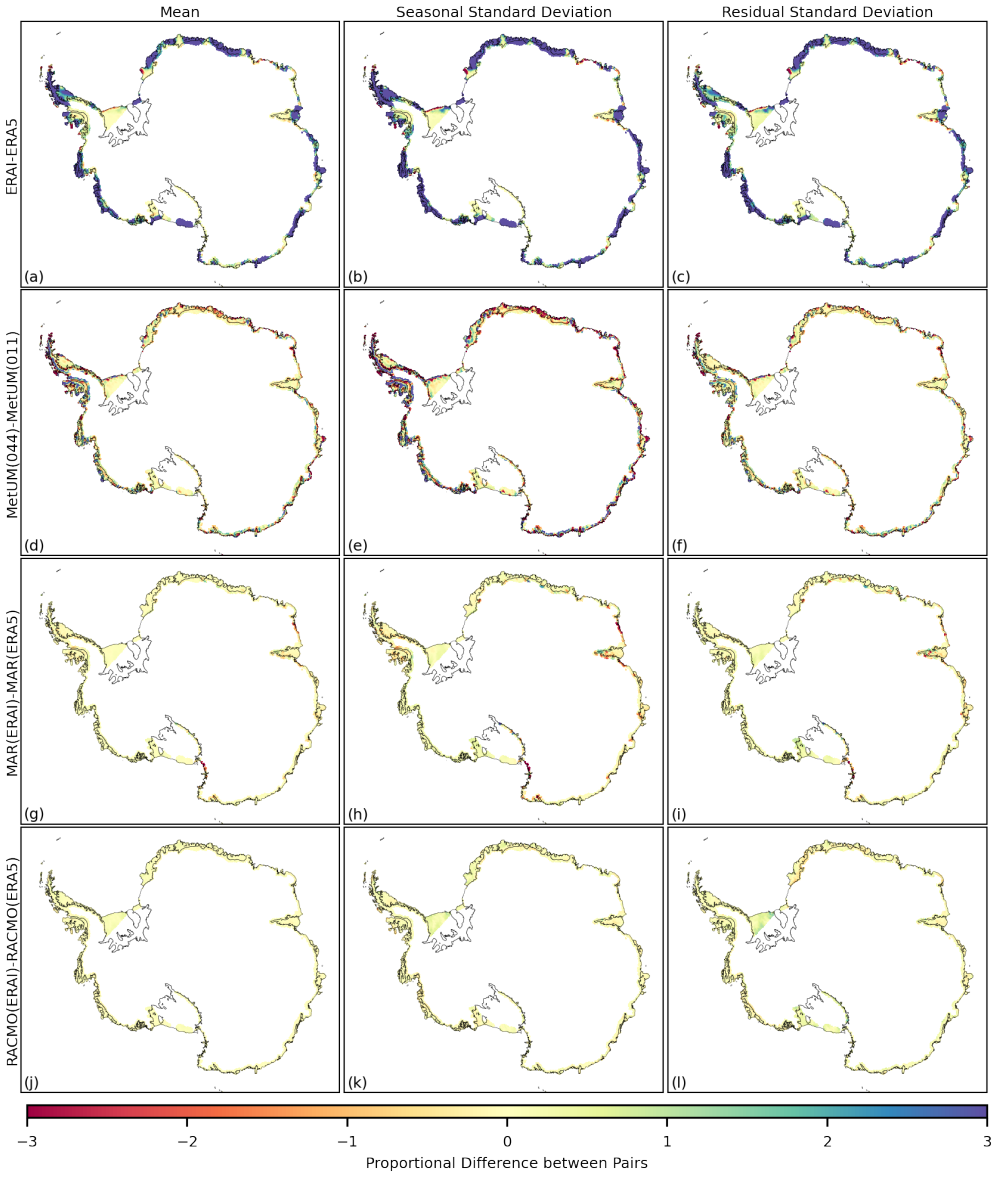

Figure B3. The difference for the 1981-2018 time series of melt, in the mean (a,d,g,j), the standard deviation of the seasonal component (b,e,h,k) and the standard deviation of the residual component (c,f,i,l) between the following pairs of outputs: ERA-Interim relative to ERA5 (a,b,c); MetUM(044) relative to MetUM(011) (d,e,f); MAR(ERAI) relative to MAR(ERA5) (g,h,i); RACMO(ERAI) relative to RACMO(ERA5) (j,k,l). Differences at each grid cell are expressed as a proportion of average inter-annual variation and so do not have units. Grid-cells where the ensemble mean average monthly melt is less than 1 $mm\ w.e.\ m^{-1}$ are masked.

Appendix C: DEM Differences

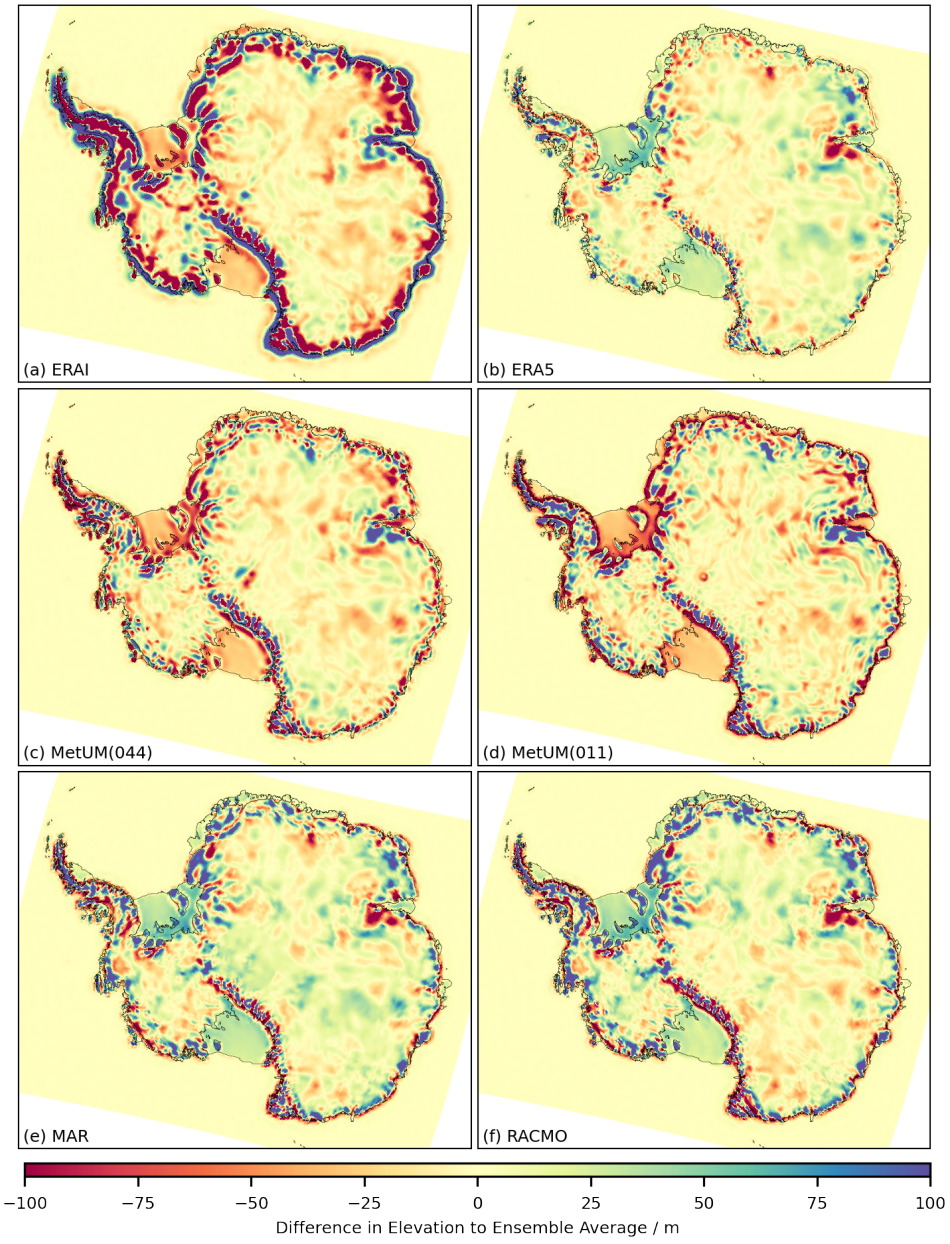

Figure C1. The difference between the DEM used by each climate model is plot relative to the ensemble average (a. ERA-Interim, b. ERA5, c. MetUM(044), d. MetUM(011), e. MAR and f. RACMO). The DEMs are regrid onto the MetUM(011) 12.5 km^2 grid for comparison. Units are meters of elevation difference.

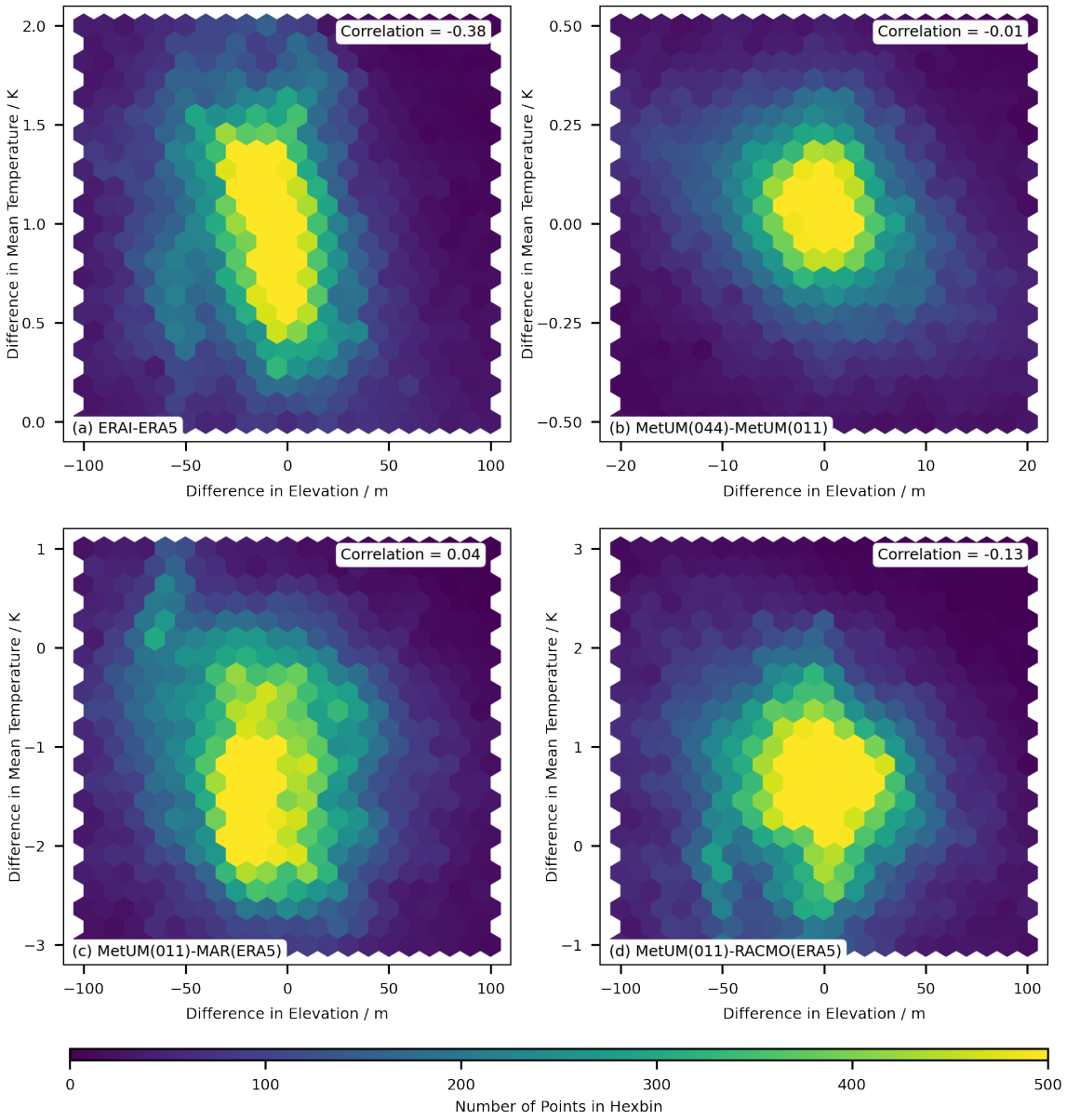

Figure C2. A density scatter plot showing the correlation between the difference in elevation for each model relative to the ensemble and the difference for near-surface temperature in the mean of the time series (a), the standard deviation of the seasonal component (b) and the standard deviation of the residual component (c). The linear Pearson correlation coefficient is given for each plot.

Author contributions. J.Carter: Conceptualization, Methodology, Software, Validation, Formal analysis, Writing - Original Draft. A.Leeson: Conceptualization, Writing - Review & Editing, Supervision. A.Orr: Conceptualization, Data Curation, Writing - Review & Editing, Supervision. C.Kittel: Data Curation, Writing - Review & Editing. J.M. van Wessem: Data Curation, Writing - Review & Editing.

Competing interests. The authors declare that they have no conflict of interest.

Acknowledgements. J.Carter is supported by the Data Science for the Natural Environment project (EPSRC grant number EP/R01860X/1). J.M. van Wessem was partly funded by the NWO (Netherlands Organisation for Scientific Research) VENI grant VI.Veni.192.083. Computational resources for MAR simulations have been provided by the Consortium des Équipements de Calcul Intensif (CÉCI), funded by the Fonds de la Recherche Scientifique de Belgique (F.R.S. – FNRS) under grant no. 2.5020.11 and the Tier-1 supercomputer (Zenobe) of the Fédération Wallonie Bruxelles infrastructure funded by the Walloon Region under grant agreement no. 1117545. C.Kittel's was supported by by the Fonds de la Recherche Scientifique – FNRS under grant no. T.0002.16 and the H2020 CRiceS. The code for analysis is written in Python 3.8.12 and makes extensive use the following libraries: Iris (Met Office, 2010); NumPy (Harris et al., 2020); Matplotlib (Hunter, 2007).

References

Agosta, C., Amory, C., Kittel, C., Orsi, A., Favier, V., Gallée, H., van den Broeke, M. R., Lenaerts, J. T. M., van Wessem, J. M., van de Berg, W. J., and Fettweis, X.: Estimation of the Antarctic surface mass balance using the regional climate model MAR (1979–2015) and identification of dominant processes, The Cryosphere, 13, 281–296, https://doi.org/https://doi.org/10.5194/tc-13-281-2019, publisher: Copernicus GmbH, 2019.

Balsamo, G., Beljaars, A., Scipal, K., Viterbo, P., Hurk, B. v. d., Hirschi, M., and Betts, A. K.: A Revised Hydrology for the ECMWF Model: Verification from Field Site to Terrestrial Water Storage and Impact in the Integrated Forecast System, Journal of Hydrometeorology, 10, 623–643, https://doi.org/10.1175/2008JHM1068.1, publisher: American Meteorological Society Section: Journal of Hydrometeorology, 2009.

Bamber, J. L., Gomez-Dans, J. L., and Griggs, J. A.: A new 1 km digital elevation model of the Antarctic derived from combined satellite radar and laser data – Part 1: Data and methods, The Cryosphere, 3, 101–111, https://doi.org/10.5194/tc-3-101-2009, publisher: Copernicus GmbH, 2009.

Bamber, J. L., Oppenheimer, M., Kopp, R. E., Aspinall, W. P., and Cooke, R. M.: Ice sheet contributions to future sea-level rise from structured expert judgment, Proceedings of the National Academy of Sciences, 116, 11 195–11 200, https://doi.org/10.1073/pnas.1817205116, publisher: National Academy of Sciences Section: Physical Sciences, 2019.

Banwell, A. F., MacAyeal, D. R., and Sergienko, O. V.: Breakup of the Larsen B Ice Shelf triggered by chain reaction drainage of supraglacial lakes, Geophysical Research Letters, 40, 5872–5876, https://doi.org/10.1002/2013GL057694, _eprint: https://agupubs.onlinelibrary.wiley.com/doi/pdf/10.1002/2013GL057694, 2013.

Bell, R. E., Banwell, A. F., Trusel, L. D., and Kingslake, J.: Antarctic surface hydrology and impacts on ice-sheet mass balance, Nature Climate Change, 8, 1044–1052, https://doi.org/10.1038/s41558-018-0326-3, wOS:000451919500014, 2018.

Best, M. J., Pryor, M., Clark, D. B., Rooney, G. G., Essery, R. L. H., Ménard, C. B., Edwards, J. M., Hendry, M. A., Porson, A., Gedney, N., Mercado, L. M., Sitch, S., Blyth, E., Boucher, O., Cox, P. M., Grimmond, C. S. B., and Harding, R. J.: The Joint UK Land Environment Simulator (JULES), model description – Part 1: Energy and water fluxes, Geoscientific Model Development, 4, 677–699, https://doi.org/10.5194/gmd-4-677-2011, publisher: Copernicus GmbH, 2011.

Bromwich, D. H.: Satellite Analyses of Antarctic Katabatic Wind Behavior, Bulletin of the American Meteorological Society, 70, 738–749, https://doi.org/10.1175/1520-0477(1989)070<0738:SAOAKW>2.0.CO;2, publisher: American Meteorological Society Section: Bulletin of the American Meteorological Society, 1989.

Brun, E., David, P., Sudul, M., and Brunot, G.: A numerical model to simulate snow-cover stratigraphy for operational avalanche forecasting, Journal of Glaciology, 38, 13–22, https://doi.org/10.1017/s0022143000009552, publisher: Cambridge University Press (CUP), 1992.

Bulthuis, K., Arnst, M., Sun, S., and Pattyn, F.: Uncertainty quantification of the multi-centennial response of the Antarctic ice sheet to climate change, Cryosphere, 13, 1349–1380, https://doi.org/10.5194/tc-13-1349-2019, wOS:000465635800003, 2019.

Bush, M., Allen, T., Bain, C., Boutle, I., Edwards, J., Finnenkoetter, A., Franklin, C., Hanley, K., Lean, H., Lock, A., Manners, J., Mittermaier, M., Morcrette, C., North, R., Petch, J., Short, C., Vosper, S., Walters, D., Webster, S., Weeks, M., Wilkinson, J., Wood, N., and Zerroukat, M.: The first Met Office Unified Model–JULES Regional Atmosphere and Land configuration, RAL1, Geoscientific Model Development, 13, 1999–2029, https://doi.org/10.5194/gmd-13-1999-2020, publisher: Copernicus GmbH, 2020.

Cape, M. R., Vernet, M., Skvarca, P., Marinsek, S., Scambos, T., and Domack, E.: Foehn winds link climate-driven warming to ice shelf evolution in Antarctica, Journal of Geophysical Research-Atmospheres, 120, 11 037–11 057, https://doi.org/10.1002/2015JD023465, wOS:000367823600001, 2015.

Carter, J.: Jez-Carter/Antarctica_Climate_Variability: 0.1.0, https://doi.org/10.5281/zenodo.6375205, 2022.

Carter, J., Leeson, A., Orr, A., Kittel, C., and van Wessem, M.: Variability in Antarctic Surface Climatology Across Regional Climate Models and Reanalysis Datasets, https://doi.org/10.5281/zenodo.6367850, type: dataset, 2022.

Christensen, J. H., Boberg, F., Christensen, O. B., and Lucas-Picher, P.: On the need for bias correction of regional climate change projections of temperature and precipitation, Geophysical Research Letters, 35, https://doi.org/10.1029/2008GL035694, _eprint: https://onlinelibrary.wiley.com/doi/pdf/10.1029/2008GL035694, 2008.

Cleveland, R. B., Cleveland, W. S., and Terpenning, I.: STL: A Seasonal-Trend Decomposition Procedure Based on Loess, p. 3, https://www.proquest.com/docview/1266805989?pq-origsite=gscholar&cbl=105444&fromopenview=true, num Pages: 3 Publisher: Statistics Sweden (SCB), 1990.

Datta, R. T., Tedesco, M., Fettweis, X., Agosta, C., Lhermitte, S., Lenaerts, J. T. M., and Wever, N.: The Effect of Foehn-Induced Surface Melt on Firn Evolution Over the Northeast Antarctic Peninsula, Geophysical Research Letters, 46, 3822–3831, https://doi.org/10.1029/2018GL080845, _eprint: https://agupubs.onlinelibrary.wiley.com/doi/pdf/10.1029/2018GL080845, 2019.

DeConto, R., Pollard, D., Alley, R., Velicogna, I., Gasson, E., Gomez, N., Sadai, S., Condron, A., Gilford, D., Ashe, E., Kopp, R., Li, D., and Dutton, A.: The Paris Climate Agreement and future sea-level rise from Antarctica, Nature, 593, 83–89, https://doi.org/10.1038/s41586-021-03427-0, 2021.

Dee, D. P., Uppala, S. M., Simmons, A. J., Berrisford, P., Poli, P., Kobayashi, S., Andrae, U., Balmaseda, M. A., Balsamo, G., Bauer, P., Bechtold, P., Beljaars, A. C. M., Berg, L. v. d., Bidlot, J., Bormann, N., Delsol, C., Dragani, R., Fuentes, M., Geer, A. J., Haimberger, L., Healy, S. B., Hersbach, H., Hólm, E. V., Isaksen, L., Kållberg, P., Köhler, M., Matricardi, M., McNally, A. P., Monge-Sanz, B. M., Morcrette, J.-J., Park, B.-K., Peubey, C., Rosnay, P. d., Tavolato, C., Thépaut, J.-N., and Vitart, F.: The ERA-Interim reanalysis: configuration and performance of the data assimilation system, Quarterly Journal of the Royal Meteorological Society, 137, 553–597, https://doi.org/10.1002/qj.828, _eprint: https://rmets.onlinelibrary.wiley.com/doi/pdf/10.1002/qj.828, 2011.

Depoorter, M. A., Bamber, J. L., Griggs, J., Lenaerts, J. T. M., Ligtenberg, S. R. M., van den Broeke, M. R., and Moholdt, G.: Antarctic masks (ice-shelves, ice-sheet, and islands), link to shape file, In supplement to: Depoorter, MA et al. (2013): Calving fluxes and basal melt rates of Antarctic ice shelves. Nature, 502, 89-92, https://doi.org/10.1038/nature12567, https://doi.org/10.1594/PANGAEA.819147, publisher: PANGAEA type: dataset, 2013.

ECMWF: IFS Documentation CY33R1, IFS Documentation, ECMWF, 2009.

ECMWF: The ERA-Interim reanalysis dataset, Copernicus Climate Change Service (C3S), https://www.ecmwf.int/en/forecasts/datasets/archive-datasets/reanalysis-datasets/era-interim, 2011.

ECMWF: IFS Documentation CY41R2, IFS Documentation, ECMWF, 2016.

Ehret, U., Zehe, E., Wulfmeyer, V., Warrach-Sagi, K., and Liebert, J.: HESS Opinions "Should we apply bias correction to global and regional climate model data?", Hydrology and Earth System Sciences, 16, 3391–3404, https://doi.org/10.5194/hess-16-3391-2012, publisher: Copernicus GmbH, 2012.

Elvidge, A. D., Sandu, I., Wedi, N., Vosper, S. B., Zadra, A., Boussetta, S., Bouyssel, F., Niekerk, A. v., Tolstykh, M. A., and Ujiie, M.: Uncertainty in the Representation of Orography in Weather and Climate Models and Implications for Parame-

terized Drag, Journal of Advances in Modeling Earth Systems, 11, 2567–2585, https://doi.org/10.1029/2019MS001661, _eprint: https://agupubs.onlinelibrary.wiley.com/doi/pdf/10.1029/2019MS001661, 2019.

Elvidge, A. D., Kuipers Munneke, P., King, J. C., Renfrew, I. A., and Gilbert, E.: Atmospheric drivers of melt on Larsen C Ice Shelf: Surface energy budget regimes and the impact of foehn, Journal of Geophysical Research: Atmospheres, 125, https://doi.org/10.1029/2020JD032463, 2020.

Ettema, J., van den Broeke, M. R., van Meijgaard, E., van de Berg, W. J., Box, J. E., and Steffen, K.: Climate of the Greenland ice sheet using a high-resolution climate model – Part 1: Evaluation, The Cryosphere, 4, 511–527, https://doi.org/10.5194/tc-4-511-2010, publisher: Copernicus GmbH, 2010.

Fettweis, X., Franco, B., Tedesco, M., van Angelen, J. H., Lenaerts, J. T. M., van den Broeke, M. R., and Gallée, H.: Estimating the Greenland ice sheet surface mass balance contribution to future sea level rise using the regional atmospheric climate model MAR, The Cryosphere, 7, 469–489, https://doi.org/10.5194/tc-7-469-2013, publisher: Copernicus GmbH, 2013.

Fettweis, X., Box, J. E., Agosta, C., Amory, C., Kittel, C., Lang, C., van As, D., Machguth, H., and Gallée, H.: Reconstructions of the 1900–2015 Greenland ice sheet surface mass balance using the regional climate MAR model, The Cryosphere, 11, 1015–1033, https://doi.org/10.5194/tc-11-1015-2017, publisher: Copernicus GmbH, 2017.

Franco, B., Fettweis, X., Lang, C., and Erpicum, M.: Impact of spatial resolution on the modelling of the Greenland ice sheet surface mass balance between 1990–2010, using the regional climate model MAR, The Cryosphere, 6, 695–711, https://doi.org/10.5194/tc-6-695-2012, publisher: Copernicus GmbH, 2012.

Fretwell, P., Pritchard, H. D., Vaughan, D. G., Bamber, J. L., Barrand, N. E., Bell, R., Bianchi, C., Bingham, R. G., Blankenship, D. D., Casassa, G., Catania, G., Callens, D., Conway, H., Cook, A. J., Corr, H. F. J., Damaske, D., Damm, V., Ferraccioli, F., Forsberg, R., Fujita, S., Gim, Y., Gogineni, P., Griggs, J. A., Hindmarsh, R. C. A., Holmlund, P., Holt, J. W., Jacobel, R. W., Jenkins, A., Jokat, W., Jordan, T., King, E. C., Kohler, J., Krabill, W., Riger-Kusk, M., Langley, K. A., Leitchenkov, G., Leuschen, C., Luyendyk, B. P., Matsuoka, K., Mouginot, J., Nitsche, F. O., Nogi, Y., Nost, O. A., Popov, S. V., Rignot, E., Rippin, D. M., Rivera, A., Roberts, J., Ross, N., Siegert, M. J., Smith, A. M., Steinhage, D., Studinger, M., Sun, B., Tinto, B. K., Welch, B. C., Wilson, D., Young, D. A., Xiangbin, C., and Zirizzotti, A.: Bedmap2: improved ice bed, surface and thickness datasets for Antarctica, The Cryosphere, 7, 375–393, https://doi.org/10.5194/tc-7-375-2013, 2013.

Gallée, H.: Simulation of the Mesocyclonic Activity in the Ross Sea, Antarctica, Monthly Weather Review, 123, 2051–2069, https://doi.org/10.1175/1520-0493(1995)123<2051:SOTMAI>2.0.CO;2, publisher: American Meteorological Society Section: Monthly Weather Review, 1995.

Gallée, H. and Gorodetskaya, I. V.: Validation of a limited area model over Dome C, Antarctic Plateau, during winter, Climate Dynamics, 34, 61, https://doi.org/10.1007/s00382-008-0499-y, 2008.

Gallée, H. and Schayes, G.: Development of a Three-Dimensional Meso-γ Primitive Equation Model: Katabatic Winds Simulation in the Area of Terra Nova Bay, Antarctica, Monthly Weather Review, 122, 671–685, https://doi.org/10.1175/1520-0493(1994)122<0671:DOATDM>2.0.CO;2, publisher: American Meteorological Society Section: Monthly Weather Review, 1994.

Gilbert, E. and Kittel, C.: Surface Melt and Runoff on Antarctic Ice Shelves at 1.5°C, 2°C, and 4°C of Future Warming, Geophysical Research Letters, 48, e2020GL091 733, https://doi.org/10.1029/2020GL091733, _eprint: https://onlinelibrary.wiley.com/doi/pdf/10.1029/2020GL091733, 2021.

Gilbert, E., Orr, A., King, J. C., Renfrew, I. A., Lachlan-Cope, T., Field, P. F., and Boutle, I. A.: Summertime cloud phase strongly influences surface melting on the Larsen C ice shelf, Antarctica, Quarterly Journal of the Royal Meteorological Society, 146, 1575–1589, https://doi.org/https://doi.org/10.1002/qj.3753, _eprint: https://rmets.onlinelibrary.wiley.com/doi/pdf/10.1002/qj.3753, 2020.

Gilbert, E. M. K., Orr, A., King, J. C., Renfrew, I., and Lachlan-Cope, T. A.: A 20-year study of melt processes over Larsen C Ice Shelf using a high-resolution regional atmospheric model: Part 1, Model configuration and validation, https://doi.org/10.1002/essoar.10506250.1, archive Location: world Publisher: Earth and Space Science Open Archive Section: Atmospheric Sciences, 2021.

Giorgi, F.: Thirty Years of Regional Climate Modeling: Where Are We and Where Are We Going next?, Journal of Geophysical Research: Atmospheres, 124, 5696–5723, https://doi.org/10.1029/2018JD030094, _eprint: https://agupubs.onlinelibrary.wiley.com/doi/pdf/10.1029/2018JD030094, 2019.

Hansen, N., Langen, P. L., Boberg, F., Forsberg, R., Simonsen, S. B., Thejll, P., Vandecrux, B., and Mottram, R.: Downscaled surface mass balance in Antarctica: impacts of subsurface processes and large-scale atmospheric circulation, The Cryosphere, 15, 4315–4333, https://doi.org/10.5194/tc-15-4315-2021, publisher: Copernicus GmbH, 2021.

Hansen, N., Simonsen, S. B., Boberg, F., Kittel, C., Orr, A., Souverijns, N., van Wessem, J. M., and Mottram, R.: Brief communication: Impact of common ice mask in surface mass balance estimates over the Antarctic ice sheet, The Cryosphere, 16, 711–718, https://doi.org/10.5194/tc-16-711-2022, publisher: Copernicus GmbH, 2022.

Harris, C. R., Millman, K. J., van der Walt, S. J., Gommers, R., Virtanen, P., Cournapeau, D., Wieser, E., Taylor, J., Berg, S., Smith, N. J., Kern, R., Picus, M., Hoyer, S., van Kerkwijk, M. H., Brett, M., Haldane, A., del Río, J. F., Wiebe, M., Peterson, P., Gérard-Marchant, P., Sheppard, K., Reddy, T., Weckesser, W., Abbasi, H., Gohlke, C., and Oliphant, T. E.: Array programming with NumPy, Nature, 585, 357–362, https://doi.org/10.1038/s41586-020-2649-2, number: 7825 Publisher: Nature Publishing Group, 2020.

Heinemann, G. and Zentek, R.: A Model-Based Climatology of Low-Level Jets in the Weddell Sea Region of the Antarctic, Atmosphere, 12, 1635, https://doi.org/10.3390/atmos12121635, number: 12 Publisher: Multidisciplinary Digital Publishing Institute, 2021.

Hersbach, H., Bell, B., Berrisford, P., Biavati, G., Horányi, A., Muñoz Sabater, J., Nicolas, J., Peubey, C., Radu, R., Rozum, I., Schepers, D., Simmons, A., Soci, C., Dee, D., and Thépaut, J.-N.: ERA5 hourly data on pressure levels from 1979 to present. Copernicus Climate Change Service (C3S) Climate Data Store (CDS)., https:/doi.org/10.24381/cds.bd0915c6, 2018.

Hersbach, H., Bell, B., Berrisford, P., Hirahara, S., Horányi, A., Muñoz-Sabater, J., Nicolas, J., Peubey, C., Radu, R., Schepers, D., Simmons, A., Soci, C., Abdalla, S., Abellan, X., Balsamo, G., Bechtold, P., Biavati, G., Bidlot, J., Bonavita, M., Chiara, G. D., Dahlgren, P., Dee, D., Diamantakis, M., Dragani, R., Flemming, J., Forbes, R., Fuentes, M., Geer, A., Haimberger, L., Healy, S., Hogan, R. J., Hólm, E., Janisková, M., Keeley, S., Laloyaux, P., Lopez, P., Lupu, C., Radnoti, G., Rosnay, P. d., Rozum, I., Vamborg, F., Villaume, S., and Thépaut, J.-N.: The ERA5 global reanalysis, Quarterly Journal of the Royal Meteorological Society, 146, 1999–2049, https://doi.org/10.1002/qj.3803, _eprint: https://rmets.onlinelibrary.wiley.com/doi/pdf/10.1002/qj.3803, 2020.

Hunter, J. D.: Matplotlib: A 2D Graphics Environment, Computing in Science Engineering, 9, 90–95, https://doi.org/10.1109/MCSE.2007.55, conference Name: Computing in Science Engineering, 2007.

Kittel, C., Amory, C., Agosta, C., Jourdain, N. C., Hofer, S., Delhasse, A., Doutreloup, S., Huot, P.-V., Lang, C., Fichefet, T., and Fettweis, X.: Diverging future surface mass balance between the Antarctic ice shelves and grounded ice sheet, The Cryosphere, 15, 1215–1236, https://doi.org/10.5194/tc-15-1215-2021, publisher: Copernicus GmbH, 2021.

Kopp, R. E., DeConto, R. M., Bader, D. A., Hay, C. C., Horton, R. M., Kulp, S., Oppenheimer, M., Pollard, D., and Strauss, B. H.: Evolving Understanding of Antarctic Ice-Sheet Physics and Ambiguity in Probabilistic Sea-Level Projections, Earth's Future, 5, 1217–1233, https://doi.org/10.1002/2017EF000663, _eprint: https://agupubs.onlinelibrary.wiley.com/doi/pdf/10.1002/2017EF000663, 2017.

Kuipers Munneke, P., Ligtenberg, S. R. M., van den Broeke, M. R., and Vaughan, D. G.: Firn air depletion as a precursor of Antarctic ice-shelf collapse, Journal of Glaciology, 60, 205–214, https://doi.org/10.3189/2014JoG13J183, wOS:000336198100001, 2014.

Lenaerts, J. T. M., van den Broeke, M. R., Déry, S. J., König-Langlo, G., Ettema, J., and Munneke, P. K.: Modelling snowdrift sublimation on an Antarctic ice shelf, The Cryosphere, 4, 179–190, https://doi.org/10.5194/tc-4-179-2010, publisher: Copernicus GmbH, 2010.

Lenaerts, J. T. M., van den Broeke, M. R., Dery, S. J., van Meijgaard, E., van de Berg, W. J., Palm, S. P., and Rodrigo, J. S.: Modeling drifting snow in Antarctica with a regional climate model: 1. Methods and model evaluation, Journal of Geophysical Research-Atmospheres, 117, D05 108, https://doi.org/10.1029/2011JD016145, wOS:000301498000002, 2012a.

Lenaerts, J. T. M., van den Broeke, M. R., van de Berg, W. J., van Meijgaard, E., and Munneke, P. K.: A new, high-resolution surface mass balance map of Antarctica (1979-2010) based on regional atmospheric climate modeling, Geophysical Research Letters, 39, L04 501, https://doi.org/10.1029/2011GL050713, wOS:000300794400004, 2012b.

Lenaerts, J. T. M., Lhermitte, S., Drews, R., Ligtenberg, S. R. M., Berger, S., Helm, V., Smeets, C. J. P. P., van den Broeke, M. R., van de Berg, W. J., van Meijgaard, E., Eijkelboom, M., Eisen, O., and Pattyn, F.: Meltwater produced by wind-albedo interaction stored in an East Antarctic ice shelf, Nature Climate Change, 7, 58–+, https://doi.org/10.1038/NCLIMATE3180, wOS:000396346700016, 2017.

Luckman, A., Elvidge, A., Jansen, D., Kulessa, B., Munneke, P. K., King, J., and Barrand, N. E.: Surface melt and ponding on Larsen C Ice Shelf and the impact of fohn winds, Antarctic Science, 26, 625–635, https://doi.org/10.1017/S0954102014000339, wOS:000344736100005, 2014.

Mann, S.: Cubic precision Clough-Tocher interpolation, Computer Aided Geometric Design, 16, 85–88, https://doi.org/10.1016/S0167-8396(98)00038-7, 1999.

Matsuoka, K., Skoglund, A., Roth, G., de Pomereu, J., Griffiths, H., Headland, R., Herried, B., Katsumata, K., Le Brocq, A., Licht, K., Morgan, F., Neff, P. D., Ritz, C., Scheinert, M., Tamura, T., Van de Putte, A., van den Broeke, M., von Deschwanden, A., Deschamps-Berger, C., Van Liefferinge, B., Tronstad, S., and Melvær, Y.: Quantarctica, an integrated mapping environment for Antarctica, the Southern Ocean, and sub-Antarctic islands, Environmental Modelling & Software, 140, 105 015, https://doi.org/10.1016/j.envsoft.2021.105015, 2021.

Met Office: Iris: A Python library for analysing and visualising meteorological and oceanographic data sets, http://scitools.org.uk/, 2010.

Mottram, R., Hansen, N., Kittel, C., van Wessem, J. M., Agosta, C., Amory, C., Boberg, F., van de Berg, W. J., Fettweis, X., Gossart, A., van Lipzig, N. P. M., van Meijgaard, E., Orr, A., Phillips, T., Webster, S., Simonsen, S. B., and Souverijns, N.: What is the surface mass balance of Antarctica? An intercomparison of regional climate model estimates, The Cryosphere, 15, 3751–3784, https://doi.org/10.5194/tc-15-3751-2021, publisher: Copernicus GmbH, 2021.

Munneke, P. K., Broeke, M. R. v. d., Lenaerts, J. T. M., Flanner, M. G., Gardner, A. S., and Berg, W. J. v. d.: A new albedo parameterization for use in climate models over the Antarctic ice sheet, Journal of Geophysical Research: Atmospheres, 116, https://doi.org/10.1029/2010JD015113, _eprint: https://agupubs.onlinelibrary.wiley.com/doi/pdf/10.1029/2010JD015113, 2011.

Orr, A., Phillips, T., Webster, S., Elvidge, A., Weeks, M., Hosking, S., and Turner, J.: Met Office Unified Model high-resolution simulations of a strong wind event in Antarctica, Quarterly Journal of the Royal Meteorological Society, 140, 2287–2297, https://doi.org/10.1002/qj.2296, _eprint: https://onlinelibrary.wiley.com/doi/pdf/10.1002/qj.2296, 2014.

Orr, A., Kirchgaessner, A., King, J., Phillips, T., Gilbert, E., Elvidge, A., Weeks, M., Gadian, A., Kuipers Munneke, P., van den Broeke, M., Webster, S., and McGrath, D.: Comparison of kilometre and sub-kilometre scale simulations of a foehn wind event over the Larsen C Ice Shelf, Antarctic Peninsula using the Met Office Unified Model (MetUM), Quarterly Journal of the Royal Meteorological Society, 147, 3472–3492, https://doi.org/10.1002/qj.4138, _eprint: https://onlinelibrary.wiley.com/doi/pdf/10.1002/qj.4138, 2021.

Paolo, F. S., Fricker, H. A., and Padman, L.: Volume loss from Antarctic ice shelves is accelerating, Science, 348, 327–331, https://doi.org/10.1126/science.aaa0940, publisher: American Association for the Advancement of Science Section: Report, 2015.

Parish, T. R. and Bromwich, D. H.: Reexamination of the Near-Surface Airflow over the Antarctic Continent and Implications on Atmospheric Circulations at High Southern Latitudes, Monthly Weather Review, 135, 1961–1973, https://doi.org/10.1175/MWR3374.1, publisher: American Meteorological Society Section: Monthly Weather Review, 2007.

Pollard, D., DeConto, R., and Alley, R.: Potential Antarctic Ice Sheet retreat driven by hydrofracturing and ice cliff failure, Earth and Planetary Science Letters, 412, https://doi.org/10.1016/j.epsl.2014.12.035, 2015.

Pritchard, H., Ligtenberg, S., Fricker, H., Vaughan, D., Van den Broeke, M., and Padman, L.: Antarctic ice-sheet loss driven by basal melting of ice shelves, Nature, 484, 502–5, https://doi.org/10.1038/nature10968, 2012.

Rignot, E., Casassa, G., Gogineni, P., Krabill, W., Rivera, A., and Thomas, R.: Accelerated ice discharge from the Antarctic Peninsula following the collapse of Larsen B ice shelf, Geophysical Research Letters, 31, https://doi.org/10.1029/2004GL020697, _eprint: https://agupubs.onlinelibrary.wiley.com/doi/pdf/10.1029/2004GL020697, 2004.

Scambos, T. A., Hulbe, C., Fahnestock, M., and Bohlander, J.: The link between climate warming and break-up of ice shelves in the Antarctic Peninsula, Journal of Glaciology, 46, 516–530, https://doi.org/10.3189/172756500781833043, publisher: Cambridge University Press, 2000.

Scambos, T. A., Bohlander, J. A., Shuman, C. A., and Skvarca, P.: Glacier acceleration and thinning after ice shelf collapse in the Larsen B embayment, Antarctica, Geophysical Research Letters, 31, https://doi.org/10.1029/2004GL020670, _eprint: https://onlinelibrary.wiley.com/doi/pdf/10.1029/2004GL020670, 2004.

Slater, A. G., Lawrence, D. M., and Koven, C. D.: Process-level model evaluation: a snow and heat transfer metric, The Cryosphere, 11, 989–996, https://doi.org/10.5194/tc-11-989-2017, publisher: Copernicus GmbH, 2017.

Tedesco, M., Doherty, S., Fettweis, X., Alexander, P., Jeyaratnam, J., and Stroeve, J.: The darkening of the Greenland ice sheet: trends, drivers, and projections (1981–2100), The Cryosphere, 10, 477–496, https://doi.org/10.5194/tc-10-477-2016, publisher: Copernicus GmbH, 2016.

Trusel, L. D., Frey, K. E., Das, S. B., Karnauskas, K. B., Munneke, P. K., van Meijgaard, E., and van den Broeke, M. R.: Divergent trajectories of Antarctic surface melt under two twenty-first-century climate scenarios, Nature Geoscience, 8, 927–U56, https://doi.org/10.1038/NGEO2563, wOS:000367200200014, 2015.

Undén, P., Rontu, L., Järvinen, H., Lynch, P., Calvo-Sanchez, J., Cats, G., Cuxart, J., Eerola, K., Fortelius, C., and García-Moya, J.: HIRLAM-5 scientific documentation, 2002.

van den Broeke, M.: Strong surface melting preceded collapse of Antarctic Peninsula ice shelf, Geophysical Research Letters, 32, https://doi.org/10.1029/2005GL023247, _eprint: https://agupubs.onlinelibrary.wiley.com/doi/pdf/10.1029/2005GL023247, 2005.

Van Meijgaard, E., Van Ulft, L. H., Van de Berg, W. J., Bosvelt, F. C., Van den Hurk, B., Lenderink, G., and Siebesma, A. P.: The KNMI regional atmospheric model RACMO version 2.1, Tech. Note Tech. Rep, 302, 2008.

van Wessem, J. M., Ligtenberg, S. R. M., Reijmer, C. H., van de Berg, W. J., van den Broeke, M. R., Barrand, N. E., Thomas, E. R., Turner, J., Wuite, J., Scambos, T. A., and van Meijgaard, E.: The modelled surface mass balance of the Antarctic Peninsula at 5.5km horizontal resolution, Cryosphere, 10, 271–285, https://doi.org/10.5194/tc-10-271-2016, wOS:000377602600017, 2016.

van Wessem, J. M., van de Berg, W. J., Noël, B. P. Y., van Meijgaard, E., Amory, C., Birnbaum, G., Jakobs, C. L., Krüger, K., Lenaerts, J. T. M., Lhermitte, S., Ligtenberg, S. R. M., Medley, B., Reijmer, C. H., van Tricht, K., Trusel, L. D., van Ulft, L. H., Wouters, B., Wuite, J., and van den Broeke, M. R.: Modelling the climate and surface mass balance of polar ice sheets using RACMO2 – Part 2:

Antarctica (1979–2016), The Cryosphere, 12, 1479–1498, https://doi.org/https://doi.org/10.5194/tc-12-1479-2018, publisher: Copernicus GmbH, 2018.

von Storch, H., Langenberg, H., and Feser, F.: A Spectral Nudging Technique for Dynamical Downscaling Purposes, Monthly Weather Review, 128, 3664–3673, https://doi.org/10.1175/1520-0493(2000)128<3664:ASNTFD>2.0.CO;2, publisher: American Meteorological Society, 2000.

Walters, D., Baran, A., Boutle, I., Brooks, M., Earnshaw, P., Edwards, J., Furtado, K., Hill, P., Lock, A., Manners, J., Morcrette, C., Mulcahy, J., Sanchez, C., Smith, C., Stratton, R., Tennant, W., Tomassini, L., Weverberg, K., Vosper, S., and Zerroukat, M.: The Met Office Unified Model Global Atmosphere 7.0/7.1 and JULES Global Land 7.0 configurations, Geoscientific Model Development, 12, 1909–1963, https://doi.org/10.5194/gmd-12-1909-2019, 2019.